This article has been accepted for publication in IEEE Access. This is the author's version which has not been fully edited and content may change prior to final publication. Citation information: DOI 10.1109/ACCESS.2026.3749135

IEEE Access
Multidisciplinary | Rapid Review | Open Access Journal

Date of publication xxxx 00, 0000, date of current version xxxx 00, 0000.

Digital Object Identifier 10.1109/ACCESS.2024.0429000

Pseudo-Haptics for Rover Teleoperation Enhanced Traction Loss Situation Awareness

RUI XAVIER[1,2], JOÃO BATISTA[1,2], JESSICA CORUJEIRA[3,4], JOSÉ LUÍS SILVA[3], and RODRIGO VENTURA[1,2] (Member, IEEE)

[1]Instituto Superior Técnico (IST), University of Lisbon, Portugal
[2]Institute for Systems and Robotics (ISR-Lisboa), Portugal
[3]ITI/LARSyS, Instituto Universitário de Lisboa (ISCTE-IUL), Lisboa, Portugal
[4]ISEL, Polytechnic University of Lisbon, Lisbon, Portugal

Corresponding author: Rui Xavier (e-mail: rui.dias.xavier@gmail.com)

This work was supported in part by FCT projects: 10.54499/LA/P/0083/2020 UID/50009/2025.

ABSTRACT Teleoperation of Unmanned Ground Vehicles (UGVs) in hazardous environments is significantly constrained by the operator's limited Situation Awareness (SA) regarding locomotion disturbances such as wheel slippage, lateral sliding, and vehicle-stuck states). These subtle physical interactions are often imperceptible through conventional video streams, risking critical mission failure. Active force-feedback haptic interfaces mitigate this, but require the introduction of significant hardware complexity and stability challenges. To overcome these constraints, we propose a novel visual-perceptual approach using Pseudo-Haptic Techniques (PHT) to convey physical vehicle-terrain forces without active force-feedback haptic devices. The primary contributions of this work are: (i) the design, implementation, and integration of three novel PHT visual metaphors (rover wheel dynamics virtual cue representation, screen peripheral border manipulation, and dynamic particle virtual cues flow); (ii) an experimental user study (with 32 participants) linking physical UGV locomotion disturbances directly to real-time PHT visual effects dynamics; (iii) a comprehensive user study evaluating both objective SA performance (disturbance detection and accuracy across Endsley's perception and comprehension levels) and subjective workload (via NASA-TLX). Statistical results demonstrate that all PHT metaphors significantly enhanced the detection of subtle traction loss compared to standard video feeds, while maintaining equivalent subjective workload and physical discomfort levels. These findings indicate that PHT offers a possible robust, software-defined, low-cost, and stability-safe alternative for enhancing SA in remote robotic operation.

INDEX TERMS human–computer interaction, human-robot interaction, pseudo-haptics, robotic teleoperation, situation awareness.

I. INTRODUCTION

ROBOTIC teleoperation involves remotely driving and manipulating robotic systems, where the operator and robot may not be in the same environment and in non line-of-sight (as illustrated in Fig. 1, by positioning a visual barrier). It has applications in space exploration, underwater inspection, planetary robotics, and hazardous environments. As robotic systems are increasingly deployed in critical domains where human lives and/or significant investments are at stake, it is crucial to ensure that operators can make informed, accurate, and timely decisions through improved situation awareness (SA) [1]. SA is a person's perception and comprehension of the elements state in the environment, at a certain time, and the projection of their state in the near future [2]. Insufficient SA can result in reduced task performance, increased error rates, and even mission failure. SA is critical for task success, especially in unstructured or dynamic environments where direct human intervention is limited or impossible.

In the context of physical separation between the operator and the robot, achieving effective SA is difficult owing to inherently limited sensory feedback. Operators primarily rely on camera feeds, which often provide a narrow field of view (FoV), insufficient depth perception, and incomplete environmental context. These visual constraints make it challenging to detect obstacles or perceive terrain irregularities, often leading to critical failures, such as wheel slippage, loss of traction, vehicle stuck states, soil sinkage, or even vehicle overturning [2], which are common mobility hazards in plan-

This work is licensed under a Creative Commons Attribution 4.0 License. For more information, see https://creativecommons.org/licenses/by/4.0/

This article has been accepted for publication in IEEE Access. This is the author's version which has not been fully edited and
content may change prior to final publication. Citation information: DOI 10.1109/ACCESS.2026.3749135

etary and extreme terrain teleoperation [3], [4]. However, those challenges are not only visual. These locomotion failures are physical events that are naturally perceived through touch and physical forces when directly driving a vehicle. Consequently, the absence of haptic feedback represents a major challenge in teleoperation [5]. Without this sensory channel, operators lose the ability to intuitively comprehend robot-environment interactions, such as surface friction or the resistive forces acting on the robot. This deprivation, forces operators to rely solely on visual inference for physical states, compromising SA in three key ways: i) reduced perception of contact forces or object resistance [6]; ii) difficulty in estimating the mechanical state of the robot [7]; and iii) increased cognitive load as operators must mentally determine physical interactions that would otherwise be felt [8] [9]. While traditional haptic feedback can close these gaps by allowing operators to sense remote interactions [10], by providing natural and intuitive control [11], this can be impractical for some robot missions. Force-feedback haptic device relies on active hardware actuators (e.g., force-reflecting joysticks or wearable suits) that physically exert real forces, torques, or vibrations directly onto the operator's body. In contrast, the techniques explored in this work do not apply direct physical forces. Instead, we utilize Pseudo-Haptic Techniques (PHT), which leverage visual force rendering, by manipulating visual feedback (such as Control/Display ratio distortions [15] and visual cues) in response to physical interaction telemetry. It aims to create a perceptual haptic illusion of friction, traction loss, or resistance directly through a standard visual display.

Despite the importance of traction awareness, current systems lack a means to convey tactile information over long distances without complex, expensive, and fragile haptic hardware. This creates a sensory gap where operators must rely on cognitively demanding visual interpretations of subtle physical events. We propose that PHT can bridge this gap by leveraging the human brain's ability to *feel* haptics through visual manipulation [12]. PHT can create a haptic sensation illusion by manipulating multimodal feedback (primarily visual) to exploit the brain's perceptual limitations [12]. By introducing distortions in the Control/Display (C/D) ratio and mapping them to user actions, PHT induces virtual tactile and kinesthetic sensations (e.g., *sticky* widgets or magnetic attraction [17]) without physical haptic devices. Unlike traditional haptics, PHT can offer a scalable, software-defined solution to simulate the sensation of traction loss, transforming purely visual feedback into a rich, multi-sensory experience. To the best of the authors' knowledge, this work presents the first comprehensive exploration of PHT specifically tailored to the unique kinematic constraints of rover locomotion. This paper examines how to enhance SA during traction-related disturbances, often the primary cause of mission-ending rover immobilizations. Our research contributes to the state-of-the-art by investigating how C/D ratio distortions (traditionally used for hand movements or virtual walking) can be mapped to robotic locomotion. The contributions of this work are:

- A Novel PHT Framework for Rover Locomotion: The conceptualization, system architecture, and implementation of three PHT metaphors designed to encode traction and sliding forces into visual feedback.
- Validation via Physical Teleoperation: A systematic user study ($N = 32$) conducted on a real rover platform, evaluating PHT effectiveness under authentic teleoperation constraints.
- SA Performance Analysis: A detailed statistical evaluation demonstrating significant improvements in Endsley's Level 1 (Perception) and Level 2 (Comprehension) SA and cognitive workload.

This paper begins with a review of related work (Section II). It then introduces the PHT concept design and proposes a system block diagram in Section III, which represents one of the main contributions of this paper. The section IV describes the implementation details and considerations. Finally, the paper presents the conducted systematic user study (section V), the obtained results (section VI), its discussion (section VII), and concludes with key findings (section VIII).

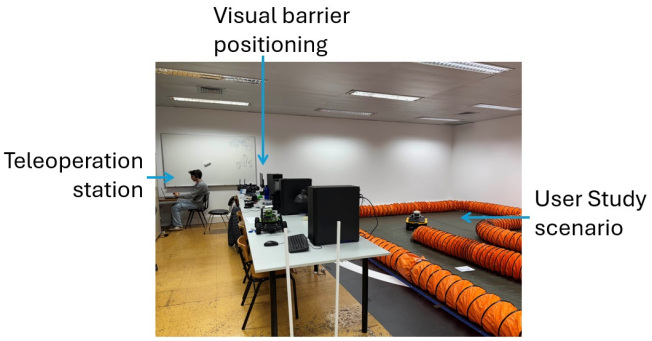


FIGURE 1. Robotic teleoperation set-up (user control station, sending commands and receiving sensor feedback from robot) and SA challenges (out-of-site / out-of-sight gap). Laboratory overview scene with a participant in the teleoperation station (with noise cancellation headphones), interacts with an interface to control an unmanned ground vehicle (with an onboard camera) in a remote environment.

II. RELATED WORK

Teleoperation of robotic vehicles poses numerous challenges, including communication latency, limited situation awareness, bandwidth constraints, and control issues [20]. The lack of SA when the unmanned ground vehicle (UGV) loses traction can lead to an incorrect and inefficient response to the current UGV state and may confuse and frustrate the human operator [21], [22]. Traction losses may occur due to irregularities in the surface plane, on a slope, the steepness of a ramp, or an incline. In unstructured space and planetary robotics domains, locomotion hazards such as wheel slippage, soil sinkage, and vehicle immobilization (stuck states) present critical risks that stall mission progress [3] [4]. Limited SA of the sliding and pushing forces impacts the operator's local navigation, may affect the ability to understand the environment and maneuver, in constrained or difficult situations [21]. It compromises teleoperation SA

This work is licensed under a Creative Commons Attribution 4.0 License. For more information, see https://creativecommons.org/licenses/by/4.0/

This article has been accepted for publication in IEEE Access. This is the author's version which has not been fully edited and
content may change prior to final publication. Citation information: DOI 10.1109/ACCESS.2026.3749135

by physically detaching the operator's intended action from the UGV response [22].

Humans naturally perceive haptic sensations when manipulating physical objects, and replicating this capability in teleoperation systems is essential for intuitive control [23]. The absence of tactile cues and the need for naturalness pose significant challenges [29]. Thus, haptic feedback has been recognized as a key enabler for addressing gaps and challenges in robotic teleoperation, where haptic feedback improves operator performance, safety, and SA [24]. Particularly, by enhancing SA critical components through improved perception of dynamic forces and environmental comprehension. To handle complex environment interaction, recent teleoperation studies have introduced advanced control and estimation strategies, such as unified contact models and hybrid motion/force control in unknown environments [25], high-order finite-time observers for sensorless interaction force estimation [26], and shared control frameworks with constrained optimization and guiding force feedback for teleoperated manipulators [27]. Haptic interfaces extend traditional display-based human–computer interaction by incorporating the sense of touch [28], particularly evident in robotic teleoperation applications. For example, in UGV teleoperation traction awareness through haptic feedback [30], for underwater robot teleoperation sensory augmentation based on VR and haptic simulators [31], a force feedback device to help teleoperation safely fly aerial Uncrewed Aerial Vehicle (UAVs) [32], an arm-wrist haptic sleeve for drone teleoperation [33], or a space flight vibrotactile feedback for spatial disorientation [34]. Indeed, providing force feedback is usually associated with haptic devices (HD). However, these haptic devices can limit users' motion and impose restrictive portability constraints [19]. Such haptic devices may also generate unintended noise, such as mechanical noise, and require frequent maintenance, introducing complexity to the interface's set-up [12]. Furthermore, HD retain a fixed physical shape and appearance regardless of function, constraining their flexibility in conveying different haptic feedback [37].

In contrast, alternative approaches have emerged to convey haptic-like sensations, particularly in VR environments and the gaming industry, commonly referred to as pseudo-haptics. They intend to simulate a haptic sensation, e.g., by combining the forces the user applies to engage the virtual environment with incongruent visual information from the simulation [15]. While direct haptics actively transmits mechanical force, e.g., back to the user's hand, using motorized devices, pseudo-haptic methods represent software-based approaches that transform estimated interaction forces, slippage, or terramechanic parameters into visual displays (e.g., visual cues) to perceive such force. PHT simulates the perceived physical properties without applying physical haptic forces.

In recent years, the number of publications on pseudo-haptics has increased significantly, reflecting a broader range of techniques and new application areas, with a focus on extended reality and mid-air interactions [38]. For instance, to feel a virtual object's weight [13] or to sense the pressure of a virtual flowing river [14]. In this case, the intended effect is achieved by manipulating visual gain, i.e., by varying the mapping ratio between virtual displacement and real-world movement [15]. This Control/Display ratio distortion will affect the user's perception of an object's speed and body movements, e.g., when walking [16], in hand movements [17], or perceiving an object's elasticity (the vertical compression Poisson effect [18]). One key advantage of pseudo-haptics over haptic devices is their device-free nature and software-defined dynamic properties, which make the interfaces more flexible and portable by enabling the dynamic modification of the virtual properties of objects [13] [18], surfaces [15], avatars [14], or applied to virtual visual cues [57]. Also, compared to HD, PHTs offer cost advantages with better mobility, portability, reduced size and weight, lower power consumption, and fewer hardware and maintenance constraints [12]. This way, PHT allows addressing those constraints of the haptic devices.

This paper also frames PHT within ecological interface design (EID) principles by design. Ecological psychology emphasizes perception as the direct acquisition of action-relevant information from the environment [39]. EID applies these principles to complex systems by making system constraints and affordances perceptually explicit [40] [41]. With Gibson's ecological approach, successful human–robot interaction (HRI) implies that the operator should be able to directly perceive the cues from the environment that support the robot's actions [35]. To support action in an environment far from a robot operator, it is important to convey the affordances of the environment to the operator such that the operator's perceived affordances of the robot in the environment match the environment's true affordances [36].

Alongside those PHT effects, considered in our work as EID design features, are foreseen to be introduced in the human peripheral vision zone, allowing the operator to keep eyes focused on the image central zone of interest. Human vision is functionally divided into two complementary subsystems: central and peripheral vision, each supporting distinct roles in visual perception and behavioral interaction with the environment [46]. Central vision (also referred to as foveal, or macular vision) is the specialized region located at the center of the retina characterized by a high density of cone photoreceptors. This region is responsible for maximum visual acuity and fine spatial resolution, enabling the detailed analysis of objects within the central degrees of the visual field. Thus, central vision is critical for tasks that require high-resolution input, such as reading, object identification, face recognition, and precise visuomotor coordination. It also plays a dominant role in color discrimination and depth perception under photopic (well-lit) conditions [47]. In contrast, peripheral vision encompasses the visual field outside the central area of fixation. Although it lacks the high spatial resolution of the fovea due to a lower cone photoreceptor density and greater convergence of retinal ganglion cells, peripheral vision plays a crucial role in motion detection, spatial orientation, and scene gist extraction. It is particularly

This work is licensed under a Creative Commons Attribution 4.0 License. For more information, see https://creativecommons.org/licenses/by/4.0/

This article has been accepted for publication in IEEE Access. This is the author's version which has not been fully edited and
content may change prior to final publication. Citation information: DOI 10.1109/ACCESS.2026.3749135

sensitive under scotopic (low-light) conditions because of the predominance of rod photoreceptors (specialized cells in the retina that are highly sensitive to light) in the peripheral retina. Peripheral vision is essential for the rapid detection of salient stimuli and supports unconscious, preattentive processing of global scene properties. Thus, this paper leverages the peripheral vision characteristics, where the perception of the PHT features, introduced in the peripheral vision zone can be manipulated to influence a person's SA.

The next sections describe the various PHT effects developed to enhance SA robotic teleoperation in challenging situations of robot traction loss and sliding. It considers a novel PHT approach as a flexible software-defined alternative to physical haptic interfaces and leverages human peripheral vision PHT effects as an ecological interface design.

III. PHT CONCEPT DESIGN AND SYSTEM DIAGRAM

A. PHT APPROACH RESEARCH QUESTIONS

The PHT approach proposed in this study hypothesizes that introducing PHT effects can enhance teleoperation SA by influencing the operator's perception and comprehension in traction-loss and sliding scenarios. To investigate this hypothesis, the following research questions (RQs) are formulated and are explicitly aligned with Endsley's SA levels theory [2]:

- **RQ1 (SA Level 1 – Perception): Can the user reliably perceive the PHT effects being conveyed for traction-related events?**
  Rationale: This question addresses the perceptual foundation of SA. It evaluates whether operators can detect and distinguish the designed PHT cues (e.g., force-feedback patterns) that indicate traction loss or sliding conditions. Without perceptual clarity, higher-level SA processes cannot be achieved.
- **RQ2 (SA Level 2 – Comprehension): Can PHT enhance the operator's comprehension of the rover's traction status during teleoperation?**
  Rationale: Building on perceptual validation, this research question examines whether PHT cues contribute to meaningful interpretation of traction-related events. It evaluates whether operators can integrate PHT signals into their mental model of the rover's state, thereby improving their comprehension of situations involving rover sliding or traction loss.

Together, these research questions delineate the intended research objective to validate whether PHT can bridge sensory gaps in robotic teleoperation by enhancing both perception (RQ1) and comprehension (RQ2) of traction-related events. The rationale is that improved SA through PHT will enable operators to perceive and mitigate risks associated with rover mobility challenges, thereby advancing the robustness of teleoperation systems.

B. PHT AS ECOLOGICAL INTERFACE DESIGN

We propose a novel approach, where PHT is positioned as an EID-aligned design paradigm. By manipulating perceptual cues rather than symbolic representations, PHT supports affordance-based interaction and enhances SA perception and comprehension levels. In ecological psychology studies [42], typical HCI involves users performing tasks based on the physical meaning of displayed symbols, representing a complex environment through rational deductive reasoning. Rapid reaction requires direct control over the process, necessitating "transparent" display systems. The concept of transparency, introduced by "Ecological Interface Design" (EID) [40], replaces the instrument approach (single-sensor-single-indicator), which is more suitable for robot instructions than human use. EID was initially devised for industrial displays, such as those used in nuclear power plant control rooms, and aligns with ecological psychology principles, providing a comprehensive account of human behavior akin to cognitive engineering [40]. By supporting human capabilities, perceptual mechanisms, and planned actions, EID facilitates learning and problem-solving, both of which are essential for building more natural HCI systems. Furthermore, the use of PHT as an EID mechanism aims to reduce cognitive load factors [39], [40], [41], including fatigue, work overload, attention demands, engagement, and expectancy, which are critical factors in long-duration teleoperation activities.

The proposed PHT approach foresees an affordance design concept, where the PHT would be applied to the input variables, extracted from the human natural tracking of motion activities, i.e., the way our body and brain instinctively monitor and adjust movements in real time. Alongside, the PHT design could evolve to support affordance in the context of the EID by allowing the user to subconsciously decompose the information patterns of new situations into familiar affordance perceptions. The PHT as EID design features aims to convey the affordances of the environment to be naturally perceived by the operator. It would be obtained by leveraging cognitive sensorimotor memory from users' daily experience, leading to the following hypothesis formulation, rationale, and design concept:

- **Hypothesis I - loss of traction / stuck SA: It considers if by inducing a PHT visual cue vibration effect, then it would address the RQ1 and RQ2 (can the operator reliably perceive and comprehend traction-related events SA) in terms of the rover loss of traction situation.**
  PHT Rationale:
  Different PHT effects were considered to enhance SA, based on our novel approach by leveraging PHT as a natural EID affordance. The PHT, as an EID per the design rationale, can be mapped to the situation where a car is losing traction/ getting stuck: the car tends to vibrate, and the driver tends to accelerate further.
  Design Concept: This PHT design concept could be applied, for example, to a PHT virtual cue wheel element representation introduced in the image's peripheral bottom region (also associated with the real rover wheels' ground-floor zone), see Fig. 3 - image a). Which will vibrate according to the traction circumstances. Or, sim-

This work is licensed under a Creative Commons Attribution 4.0 License. For more information, see https://creativecommons.org/licenses/by/4.0/

This article has been accepted for publication in IEEE Access. This is the author's version which has not been fully edited and
content may change prior to final publication. Citation information: DOI 10.1109/ACCESS.2026.3749135

ilarly to a PHT virtual boundary peripheral border bars animation, see Fig. 3 - image b). The border size and opacity of the PHT visual cues will be manipulated to achieve the intended effect. In this case, the peripheral border bars will also vibrate, conveying the perception of being inside a car, and everything will be vibrating. The Fig. 3 - image c) represents another PHT effect, the introduction of virtual cue particles flow representation (a bubbles-like visual cues). The air bubbles flow motion manipulation intends to induce external forces perception, such as the stuck effect. From the literature, a similar PHT application, Bubble Margin [57], was designed to reduce discomfort when using a smartphone in a moving vehicle. It was implemented by Apple as an iOS feature called ''Vehicle Motion Cues''[1].

These implementations applied the PHT to convey bodies' inertia. This realization could be considered supporting this paper's PHT hypothesis of using a similar PHT particles flow visual cues approach, applied in this case for robotic teleoperation external forces (stuck, sliding, and push).

- **Hypothesis II - sliding/pushing force SA: It considers if by introducing a sliding effect in the PHT visual cue, then it would address the RQ1 and RQ2 (can the operator reliably perceive and comprehend traction-related events SA) in terms of a rover sliding/pushing force.**

  PHT Rationale: Sliding is considered a distinct case of traction loss in terms of SA. For example, an operator may encounter a sliding situation even when the robot is not actively commanded to move. The rover's wheel–terrain contact areas may lead to two distinct phenomena: longitudinal slipping (defined as relative motion in the longitudinal direction of the wheel at the contact point), and lateral sliding (defined as relative motion in the lateral direction) [43]. Both introduce velocity deviations that can compromise teleoperation performance.

  Design Concept: The proposed PHT natural EID approach addresses these challenges by dynamically manipulating visual cues within the scene visualization.

  By visualizing the PHT virtual cue wheel element representation sliding in the image (Fig. 3, image a), the operator would perceive that the rover is sliding and become naturally aware of the underlying, otherwise unseen, forces and movements. A complementary PHT effect is implemented via screen-periphery border animations, designed to evoke the human *vection* phenomenon. *Vection* is a well-known visual illusion of self-motion [44] [45]. For example, when a person is seated in a stationary car or train and perceives motion as a neighboring vehicle begins to move. In such cases, the visual system interprets the surrounding motion, while the vestibular system signals stasis, forcing the brain to reconcile conflicting inputs. This produces a temporary illusion of self-motion, such as rolling backward while remaining stationary. The same principle underlies motion simulators in amusement parks, where moving visuals induce sensations of acceleration or falling. By leveraging *vection*, the PHT virtual boundary peripheral border bars motion approach conveys a sliding perception to the operator, enhancing awareness of traction disturbances, see Fig. 3 - image b). The PHT bubbles particles motion also reacts according to the rover sliding / pushing forces, by visually moving the flow in a direction consistent with real-world external forces, see Fig. 3 - image c). This visual response creates a pseudo-haptic illusion allowing the operator to intuitively infer the rover's external force interaction.

[1]https://support.apple.com/en-mt/guide/iphone/iph55564cb22/ios [accessed 12 Jan 2026]

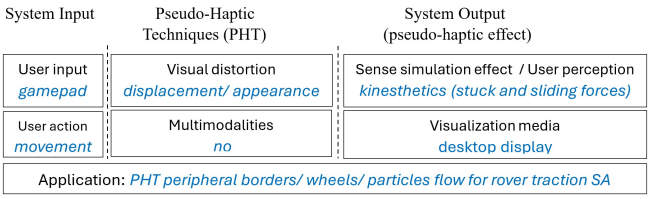


FIGURE 2. PHT block diagram for the PHTs approaches (peripheral borders, wheels representation, and particles flow visual cues) being considered for the traction loss and sliding forces teleoperation SA.

A comprehensive user study will be conducted, and the metrics collected (summarized in Table 8), to evaluate the support of the formulated hypothesis and its effectiveness in terms of teleoperation SA (SA Level 1- perceptions and SA level-2 comprehension).

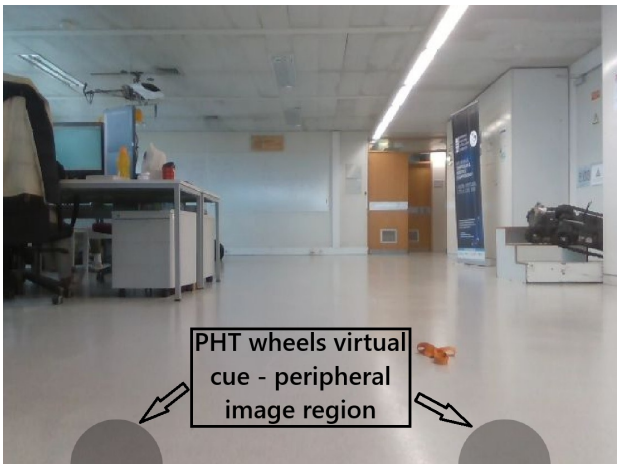
C. PHT SYSTEM BLOCK DIAGRAM

Fig. 2 shows the PHT system block diagram for the traction-loss and sliding-forces teleoperation SA. The adoption of this generic framework [38] was used for all three PHT (the peripheral borders manipulation, and the inclusion of visual cues - the wheels representation and the particles bubbles), explored in this research work and described in the section IV. The diagram block elements describe how people perceive a sense simulation effect, primarily obtained by observing stimuli and using a visual distortion technique, in a given visualization medium. It is evoked by directly mapping the PHT distortion effect with the user action input. In this case, the robot *movement* is controlled via a *gamepad*, which serves as the PHT system input. The PHT consisted of the visual cues introduced in the scene (peripheral borders, wheel representation, and particle flow). Those will be manipulated by *appearance* distortion (e.g., opacity changes and size variations) and *displacement* (e.g., by sliding the visual cue representations in the scene). The PHT system output aims to induce in the user's perception the sense of simulation of *kinesthetic* forces, such as stuck and sliding forces (loss of traction), visualized on the *desktop display*.

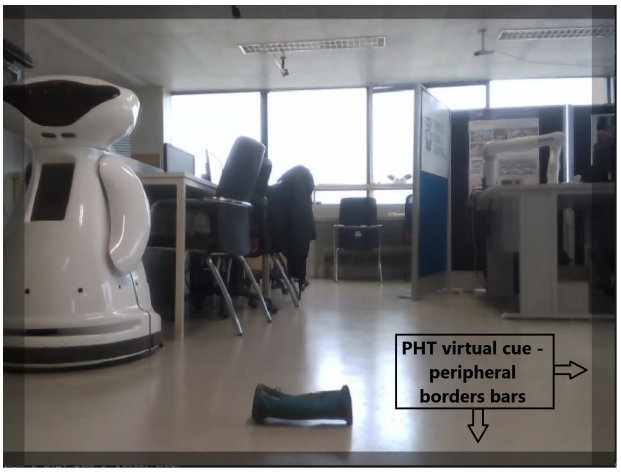
This work is licensed under a Creative Commons Attribution 4.0 License. For more information, see https://creativecommons.org/licenses/by/4.0/

This article has been accepted for publication in IEEE Access. This is the author's version which has not been fully edited and
content may change prior to final publication. Citation information: DOI 10.1109/ACCESS.2026.3749135

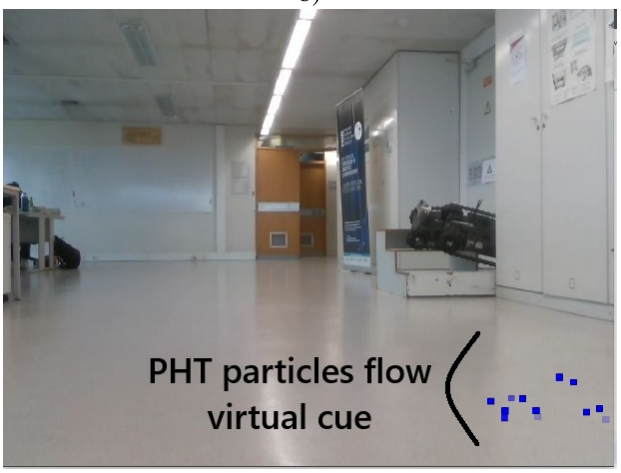
D. PHT EXPLORING HUMAN PERIPHERAL VISION



a)



b)



c)

FIGURE 3. PHT peripheral vision region feasibility study. Image a) PHT wheels virtual cue introduced in the image's peripheral bottom region (wheel size and level of capacity will be manipulated according to the intended effect). Image b) PHT boundary peripheral border bars virtual cue (border size and level of opacity will be manipulated according to the intended effect). Image c) PHT particles virtual cue flow representation (a bubbles-like visual cues), where the air bubbles motion flow manipulation intends to induce external forces perception.

The adopted PHT design effects, shown in Fig. 3, leverage the peripheral vision zone characteristics and advantages [47]. This design approach aims to contribute to the enhancement of robotic teleoperation SA, enabling the operator to keep their eyes focused on the central zone of interest. Consequently, it prevents the operator from being distracted and having to move their central macular vision away from the target area to read specific instrument information.

E. PHT C/D RATIO MAPPING DESIGN

Control–display (C/D) ratio describes the mapping between a user's physical input (control movement) and the resulting system response or visual displacement, where intentional distortion of this ratio can alter perceived effort, resistance, or dynamics [48]. These PHT manipulation mechanisms are direct, principled modulations of the C/D ratio to encode the PHT intended effect. From literature, PHT C/D ratio mapping has been used to simulate different force sensations, such as weight, gravity, viscosity, or torque [38]. In our work, once the PHT effect is triggered, the C/D ratio design mapping and implementation approach is applied. Specifically, the PHT effect is mapped to traction loss (stuck and to the sliding conditions) detected by the rover's sensors. Manipulating the C/D ratio subsequently induces a haptic force perception. The C/D ratio mapping was tailored for each of the PHT effects (wheel visual cue representation, peripheral borders, and particle flow), which will be now described in detail.

Wheel visual cue representation. The PHT visual cue representation aims to appeal to a natural perception of the rover's wheels, through the use of two semi-circles placed at the bottom of the image, which could be associated with a real rover situation when visualizing the wheels on the ground, see Fig. 3 image a). This PHT uses the equation (1) for lateral sideways sliding, where both wheels do a sideways translation (in the x axis), according to the detected sliding direction. Whenever a forward or backward sliding happens, the wheels' representation will show a translation movement (in the y axis), according to equation (2). This translation was proportional to the UGV's detected displacement ($\boldsymbol{x}_{displacement}$ and $\boldsymbol{y}_{displacement}$), with a scale vector k.

$$\mathbf{x}_{translation} = \mathbf{x}_{source} - k_x \cdot \mathbf{x}_{displacement} \tag{1}$$

$$\mathbf{y}_{translation} = \mathbf{y}_{source} - k_y \cdot \mathbf{y}_{displacement} \tag{2}$$

In the case of sliding forward, the PHT visual cue representation will become more visible, as the wheels' translational movement moves up in the image. Conversely, when sliding backwards, the PHT wheel's representation will become less visible in the image. For both Equations, the resulting translational movements were capped to maximum and minimum values. That is, for the y translation movement, the wheels will always be shown linked to the image bottom (i.e., maximum size will be the virtual wheel total height) and the wheels will never disappear from the image bottom (minimum value), although the wheels representation will become less visible.

This work is licensed under a Creative Commons Attribution 4.0 License. For more information, see https://creativecommons.org/licenses/by/4.0/

This article has been accepted for publication in IEEE Access. This is the author's version which has not been fully edited and
content may change prior to final publication. Citation information: DOI 10.1109/ACCESS.2026.3749135

Peripheral borders. It uses the PHT concept design as EID to convey bodies' inertia applied to the peripheral borders, see Fig. 3, image b). When the robot is stuck, the C/D ratio is used to create a vibratory effect by randomly oscillating the opacity of the lower peripheral border areas (without interfering with the image's central observation zone). When the UGV slides, a sliding effect becomes apparent at the image's periphery by manipulating the border sizes. The sliding effect is achieved by manipulating the borders, which increase the border size on one side with a certain level of opacity while simultaneously decreasing it on the opposite side of the image. The C/D ratio was conveyed through the variation of the borders' sizes, where the maximum height of the borders measured in pixels ($\boldsymbol{h}_{border} = [\boldsymbol{h}_{border_x}, \boldsymbol{h}_{border_y}]$), was proportional to the UGV's velocity displacement, with a scale vector $\boldsymbol{k}$. This can be defined as in equation (3).

$$\boldsymbol{h}_{border} = k \cdot \boldsymbol{v}_{displacement} \tag{3}$$

Thus, as the UGV slid forward, the bottom border of the screen expanded until it reached its maximum height. Proportionally, the top border will start at the maximum height and decrease in size, i.e., shrink from its maximum height until it disappears entirely. Similarly, the same would apply to sideways slides along the lateral peripheral borders, inducing a sliding effect to the left or right. When the UGV is stuck, all the borders would appear and randomly change opacity.

Particle flow. It uses a similar EID concept design to convey bodies' inertia as applied in the PHT peripheral borders, but now applied to the particle flow. As with the peripheral borders condition, the PHT particles flow virtual cues are introduced when a disturbance happens, otherwise no particles are displayed. This PHT particle flow was deployed with a C/D ratio mapping between the velocity difference and the bubbles' visual-cue velocity, as shown in equation (4). It considers $\boldsymbol{v}_{bubbles} = [\boldsymbol{v}_{bubbles_x} \quad \boldsymbol{v}_{bubbles_y}]$ and a scale factor k.

$$\boldsymbol{v}_{bubbles} = k \cdot \boldsymbol{v}_{displacement} \tag{4}$$

Whenever a rover lateral slide occurred, the PHT visual cue was used to create a C/D ratio-mapped sideways bubble movement in the x-axis component, see Fig. 3, image c). The y-component of the same equation was used for both forward and backward rover slides. For the stuck case, bubbles were introduced as visual cues with a very short lifespan to create the illusion that the bubbles could not progress (getting stuck), with a timescale of milliseconds, later shown in Table 4. In terms of design, the stuck condition applied only to the x-axis, as it was considered sufficient to induce a perception of stuck and to avoid creating other, more complex bubble movements that may not be directly perceived as stuck.

IV. PHT APPROACH IMPLEMENTATION

A. PROJECT FLOWCHART

Fig. 4 depicts the flowchart of the project's software implementation to achieve the desired system architecture of the traction detection PHTs.

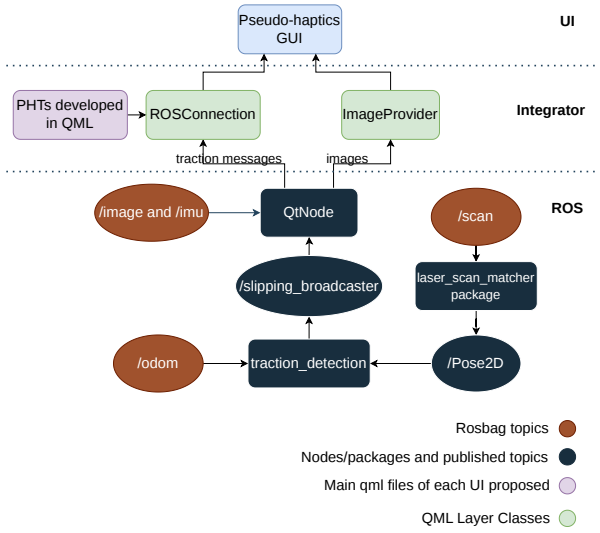


FIGURE 4. Project's ROS and QML flowchart

As shown in the Fig. 4, the system is organized into distinct layers, each responsible for specific functionalities within the overall architecture.

1) ROS Layer

This layer encompasses one package: *laser_scan_matcher*; and two nodes *traction_detection* and the *QtNode* [2]

The *laser_scan_matcher* package enables scan matching between consecutive LIDAR scans and publishes the estimated UGV position to the */Pose2D* ROS topic. The *traction_detection* node, retrieves the UGV's pose that is published by *laser_scan_matcher*, as well as the UGV's odometry [22]. It then performs cross-validation on the retrieved data and publishes the traction status on the */slipping_broadcaster* topic: whether the UGV is in normal traction conditions, slipping, or stuck. This was later extended to also send the displacement velocities along the x and y axes.

The *QtNode* serves as a mediator between the ROS and integrator layers, transmitting all relevant data retrieved from ROS to QML (Qt Meta-object Language[3]) .

2) Integrator Layer

It transmits the data retrieved from the ROS layer, via the *QtNode*, to the GUI layer, sending the camera frames through the "ImageProvider" class, and the rest of the relevant data, such as slippage cues, through the "ROSConnection" class.

3) Pseudo-haptics UI

It consists of the three PHT approaches, which were implemented in QML, as shown in Fig. 11, Fig. 12, and Fig. 13.

[2]ROS1 code – https://github.com/JoaoBatista2312/ROS1-Qt6-bridge, last accessed on 12 Sep 2026

[3]https://www.qt.io/, last accessed on 19 Oct 2025

This work is licensed under a Creative Commons Attribution 4.0 License. For more information, see https://creativecommons.org/licenses/by/4.0/

This article has been accepted for publication in IEEE Access. This is the author's version which has not been fully edited and
content may change prior to final publication. Citation information: DOI 10.1109/ACCESS.2026.3749135

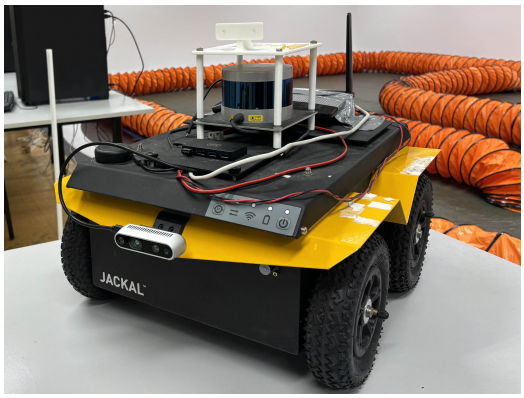


FIGURE 5. Jackal rover, a high-torque 4×4 drivetrain equipped with an IMU, wheel odometry, LIDAR, and a RealSense camera.

B. PHT TRIGGERED BY ROVER TRACTION DETECTION

For this work, a real UGV with a high-torque 4×4 drivetrain, the Jackal rover was used, as shown in Fig. 5. The Jackal, from Clearpath Robotics, is equipped with an IMU, wheel encoders, a 2D LIDAR, and an Intel RealSense camera. Rover motion was teleoperated using a Logitech Gamepad F310, connected via Wi-Fi to the teleoperation station laptop. A key advantage of this rover platform is its fused odometry capability[4], which enables the extraction of position, velocity, and acceleration estimates by combining multiple sensing modalities. This approach yields more robust motion estimates than standard wheel-encoder odometry alone and is particularly useful for detecting traction loss and sliding events.

Traction detection. Traction loss and sliding detection in this work rely on the comparison of two independent odometry estimates: (i) wheel-based odometry derived from wheel encoder measurements, and (ii) LIDAR-based odometry obtained through scan-matching against the surrounding environment. Wheel odometry estimates robot motion by measuring wheel rotations and converting them into linear and angular velocities using the robot's kinematic model. For differential-drive or skid-steered vehicles, unequal wheel velocities result in motion along a circular arc around an instantaneous center of curvature [49]. The robot's forward velocity is proportional to the average wheel speed, while its angular velocity depends on the difference between wheel speeds.

Pose displacement computation. The robot pose is defined by its position and orientation relative to a global coordinate frame [50]. The pose of the mobile robot is defined by the state vector $\mathbf{q} = [x, y, \theta]^\top$, where (x, y) represents the Cartesian coordinates of the robot's center (position on a 2D map) and θ denotes its orientation relative to the global x-axis (direction the robot is facing).

To analyze the relative motion between discrete time steps t_{k-n} and t_k, we define the incremental displacement. This relative approach is essential for isolating systematic odometry errors (such as those induced by wheel slip or surface irregularities) from absolute global drift. The discrepancy between the proprioceptive (internal sensors / wheel encoders) and exteroceptive (external sensors / LiDAR) odometry sources is quantified through the computation of the orientation displacement $\Delta\theta(t_k)$ and the local position displacement vector $\Delta\mathbf{p}(t_k)$.

The angular orientation displacement is defined as the scalar difference in heading between the start and end point, as described in the equation:

$$\Delta\theta(t_k) = \theta(t_k) - \theta(t_{k-n}), \quad \theta(t) \in [-\pi, \pi] \tag{5}$$

To achieve a robot-centric representation of movement, the global position change must be mapped into the robot's local coordinate frame. It calculates the position displacement vector $\mathbf{\Delta p}(t_k)$ in the robot's local coordinate frame, the global displacement is transformed using the transpose of the rotation matrix at the start:

$$\mathbf{\Delta p}(t_k) = \mathbf{R}^T(\theta(t_{k-n}))\,[\mathbf{p}(t_k) - \mathbf{p}(t_{k-n})] \tag{6}$$

The rotation matrix $\mathbf{R}(\theta)$, specific to the kinematics of skid-steering mobile robots [51], is defined as:

$$\mathbf{R}(\theta) = \begin{bmatrix} \cos(\theta) & -\sin(\theta) \\ \sin(\theta) & \cos(\theta) \end{bmatrix} \tag{7}$$

Odometry mismatch as traction indicator. Comparing multiple odometry sources (Proprioceptive vs. Exteroceptive) is a common method for slip detection [52]. The mismatch between wheel-based odometry and laser-based odometry is quantified by the Euclidean norm (straight-line distance from the origin) of the difference between their respective displacements (wheel-based and laser-based ground truth). The linear displacement $(\Delta x, \Delta y)$ is derived from the measured or estimated traveled distance δs and the robot's orientation θ_k. For this realization, both linear and angular displacements are computed independently using wheel odometry and LIDAR-based odometry. To quantify discrepancies between the two odometry sources, the mismatch in linear displacement and orientation is computed at each time step t_k:

$$\delta_p(t_k) = \|\mathbf{\Delta p}_{wheels}(t_k) - \mathbf{\Delta p}_{LIDAR}(t_k)\| \tag{8}$$

$$\delta_\theta(t_k) = \|\mathbf{\Delta \theta}_{wheels}(t_k) - \mathbf{\Delta \theta}_{LIDAR}(t_k)\| \tag{9}$$

where Δp_{wheels} is the displacement measured using the robot's internal wheel encoders (proprioceptive odometry), i.e., it calculates how far the robot has moved based on the rotation of its wheels. The Δp_{LIDAR} is the displacement measured using external environment sensors (exteroceptive odometry Laser Scanner).

These mismatches are then converted into linear and angular velocity displacement measures:

$$\boldsymbol{v}_{displacement} = \frac{\delta_p(t_k)}{t_k - t_{k-n}} \tag{10}$$

[4]Clearpath Robotics documentation: https://www.clearpathrobotics.com/assets/guides/noetic/jackal/JackalTests.html, last accessed on 07 Jan 2025

This work is licensed under a Creative Commons Attribution 4.0 License. For more information, see https://creativecommons.org/licenses/by/4.0/

This article has been accepted for publication in IEEE Access. This is the author's version which has not been fully edited and content may change prior to final publication. Citation information: DOI 10.1109/ACCESS.2026.3749135

TABLE 1. UGV's traction state detection and classification.

Traction state	Wheels' odometry	LIDAR odometry
Normal	Moving	Moving in the same direction
Normal	Stopped	Stopped
Stuck	Moving	Stopped
Sliding	Moving	Moving in a different direction
Sliding	Moving	Moving in same direction
Sliding	Stopped	Moving

$$\omega_{displacement} = \frac{\delta_\theta(t_k)}{t_k - t_{k-n}} \tag{11}$$

In addition to velocity magnitude discrepancies, directional differences are also considered. The velocity displacement vector is defined as:

$$\boldsymbol{v}_{displacement} = \begin{bmatrix} \boldsymbol{v}_{displacement_x} \\ \boldsymbol{v}_{displacement_y} \end{bmatrix} \tag{12}$$

A scale factor $k = [k_x \ k_y]$ is applied to tailor sensitivity for different PHT effects, allowing the system to modulate triggering thresholds according to the perceptual salience required for each cue.

Traction state classification. The mismatch between wheel odometry and LIDAR odometry serves as the primary input to determine the rover's traction state. By evaluating both velocity magnitude and direction consistency, the rover's traction status is classified into three categories: *Normal*, *Stuck*, and *Sliding*, as summarized in Table 1.

Integration with operator commands. In addition to odometry-based discrepancies, the system also considers the operator's control commands when determining traction state. Three key mismatch scenarios are explicitly handled:

- No rover movement despite control input. When the operator issues a movement command but the rover remains stationary, the situation is classified as *stuck*.
- Rover movement without control input. When the rover moves despite no user-issued command, the system detects a *sliding* state. This is critical for identifying externally induced motion, such as gravity-driven sliding.
- Discrepancy between commanded and actual motion. When the rover responds to a control command but moves in a direction inconsistent with the request, a *sliding* state is inferred. In this case, both directional mismatch and odometry disagreement are present.

A significant velocity displacement between the two odometry sources, evaluated against predefined thresholds and temporal persistence constraints, acts as the trigger input for the PHT visual effects. This ensures that PHT cues are activated only during meaningful traction-related events, providing perceptually stable and ecologically grounded feedback to enhance teleoperation situation awareness.

C. ROVER NOISE PROCESSING

A comprehensive analysis was conducted to examine the relationship between the controller input and its corresponding effect on the robot's motion. This analysis is essential for determining appropriate C/D ratios to convey the PHTs effectively. In addition, it enables the identification of the minimum sensitivity threshold required for PHT activation while minimizing false positives.

The data graphs depicted in Fig. 6 show the linear and angular velocities from both the controller command transmitted to Jackal, and the velocity the UGV took. These graphs also show the robot's acceleration curves during transitions between movements, as well as the noise error for each velocity type during the teleoperation test. Fig. 7 demonstrates the trajectory of the UGV during this analysis.

From this test, it was observed that Jackal can achieve two distinct velocity thresholds for linear and angular motion. The results are shown in Table 2. Although the Jackal robot can achieve higher velocities, with a maximum speed of 2.0 m/s, the defined rover velocities were chosen to align with the user study constraints regarding the Lab space and the user study goals.

Regarding noise values according to different velocity values, a rover noise characterization was conducted and sum-

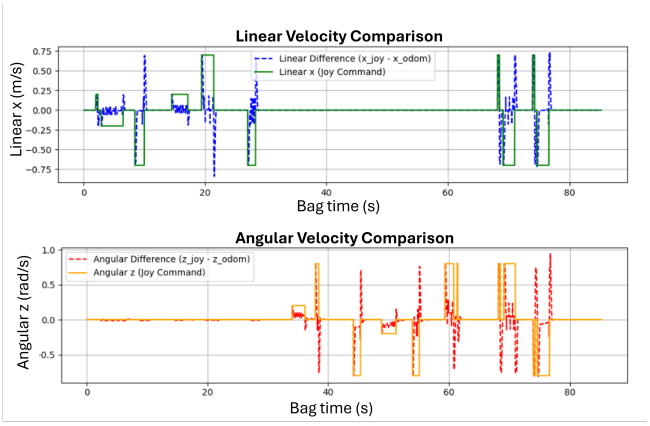


FIGURE 6. Graphic comparisons of and angular velocities

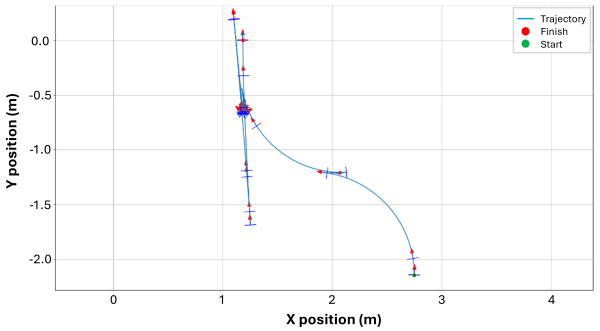


FIGURE 7. Jackal's relative trajectory

This work is licensed under a Creative Commons Attribution 4.0 License. For more information, see https://creativecommons.org/licenses/by/4.0/

This article has been accepted for publication in IEEE Access. This is the author's version which has not been fully edited and
content may change prior to final publication. Citation information: DOI 10.1109/ACCESS.2026.3749135

TABLE 2. Mapping of Jackal's movement

Velocity type	Unit used	First threshold	Second threshold
Linear (x)	m/s	0.2	0.7
Angular (z)	rad/s	0.2	0.8

marized in Table 3.

TABLE 3. Rover linear and angular velocity noise values characterization.

Velocity:	Linear (m/s)	Noise (m/s)	Angular (rad/s)	Noise (rad/s)
- Max. vel.	-0.7	0.178	-0.8	0.241
- Min. Vel.	-0.2	0.056	-0.2	0.114
Stopped	0.0	3.32E-04	0.0	0.021
+ Min. Vel.	0.2	0.061	0.2	0.099
+ Max. Vel.	0.7	0.181	0.8	0.272

To prevent the PHTs from being sensitive to noise, a threshold was defined based on the noise specifications. This input–output analysis was essential to identify the displacement thresholds best suited for Jackal. The goal was to maximize sensitivity to displacement while keeping values above the sensor noise level. Additionally, this analysis helped determine how the threshold sensitivity values should be adjusted for the Jackal's inputs.

D. PHT MINIMUM ANIMATION ACTIVATION TIME

TABLE 4. PHT minimum animation activation time.

PHTs (conditions)	Lateral sliding (ms)	Backwards sliding (ms)	Stuck (ms)
Peripheral borders	400	350	100
Wheels	400	350	100
Particles flow	1500	1000	900

The literature on human visual processing identifies a reliable temporal integration window (the time over which the visual system combines successive inputs) commonly cited as approximately 100 ms [53]. Based on this finding, the minimum activation time for PHT animations was set to 100 ms across all PHT experimental conditions. This threshold was applied consistently for rover scenarios involving both stuck and sliding states, as summarized in Table 4. The duration of PHT animations is further determined by the specific requirements of each effect's implementation. Importantly, no upper limit is imposed on the animation duration. The PHT effects are designed to persist as long as the rover artifact is detected (e.g., traction loss or sliding). This ensures that operators receive continuous perceptual cues aligned with the rover's dynamic state, supporting sustained situational awareness during teleoperation.

V. EVALUATION

A. USER STUDY DESIGN

This study involves the teleoperation of the Jackal across different locomotion scenarios. The participants traversed all

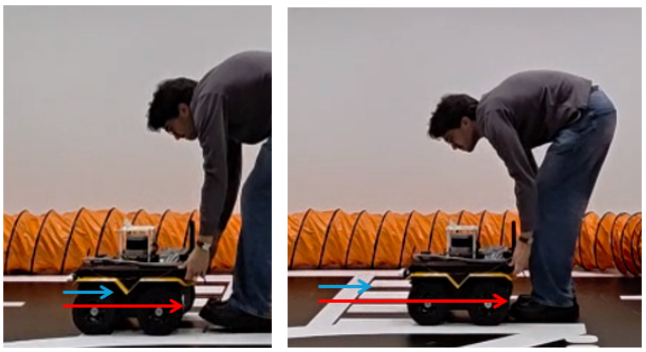


FIGURE 8. Slide backwards small and Slide backwards big



FIGURE 9. Slide lateral small and slide lateral big

possible traction states: *Normal*, *Stuck*, and *Sliding*. Because different types and magnitudes of sliding were required during the trials, the researchers of the user study artificially induced them, in an equalitarian way across all the participants. Examples of sliding behavior are shown in the following Fig. 8, 9 and 10, where the blue arrows represent the non-disturbed motion, and the red arrows represent the motion when the UGV was disturbed. The initial part of the arrows indicates where the UGV started moving, which was fully aligned with the first crosswalk line.

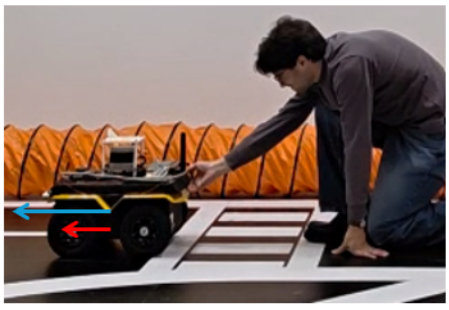


FIGURE 10. Stuck visual demonstration

The participants underwent four trials, including a control condition (only a camera display) and the implemented PHTs (peripheral borders, flow, and wheels). The way they act

This work is licensed under a Creative Commons Attribution 4.0 License. For more information, see https://creativecommons.org/licenses/by/4.0/

This article has been accepted for publication in IEEE Access. This is the author's version which has not been fully edited and
content may change prior to final publication. Citation information: DOI 10.1109/ACCESS.2026.3749135

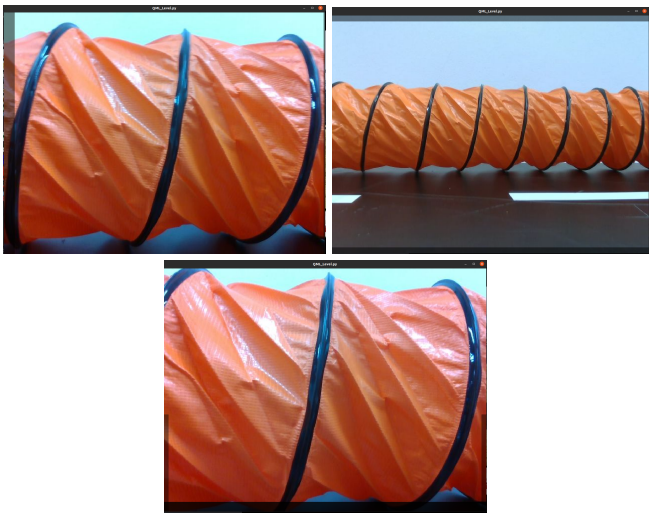


FIGURE 11. Periheral Borders visual representation of each disturbance type. The upper left Figure is a left-to-right slide, the upper right of a slide backwards and the bottom Figure of the stuck scenario.



FIGURE 12. Flow visual representation of each disturbance type. The upper left figure is a left-to-right slide, the upper right of a slide backwards and the bottom figure of the stuck scenario.

upon each disturbance type is shown in Fig. 11, Fig. 12, and Fig. 13. Each figure depicts how the PHTs act on lateral slides, backward slides, and, when the UGV is stuck, in the corresponding order.

On the Peripheral Borders, depicted in Fig. 11, a slide from left to right makes the borders increase on the right side of the periphery, while decreasing the left border's size. In Fig. 11, the frame depicted is one of the initial frames; therefore, the left border is still bigger than the right one. Sliding backwards increases the bottom border of the periphery, while decreasing the upward border's size. When stuck, it varies the bottom peripheral border, as well as half of the lateral peripheral borders' opacity, with a random opacity value. Particle flow, depicted in Fig. 12, a slide from left to right causes bubbles to appear from the left periphery toward the center of the screen.



FIGURE 13. Wheels visual representation of each disturbance type. The upper left figure is a left-to-right slide, the upper right of a slide backwards and the bottom figure of the stuck scenario.

Sliding backwards causes bubbles to appear from the bottom periphery and move toward the center of the screen. Lastly, the stuck situation causes bubbles to appear at the center of the screen with low velocity, to depict the robot struggling to move forward.

The Wheels interface, shown in Fig. 13, slides from left to right, causing the wheels to follow the UGV's movement. Sliding backwards causes the wheels to move downward. Stuck increases opacity and varies the size of the wheels at random, capped at a maximum size.

The order of the trials was randomized to reduce any carryover effects on the participants.

B. USER STUDY APPARATUS

Fig. 1 depicts the overview of the laboratory where the user study was conducted, with the teleoperation station, as well as the user study scenario.

1) Teleoperation Station

As shown in Fig. 14, the teleoperation station consisted of a small table positioned near the scenario to ensure a stable connection between the teleoperation station's laptop and Jackal itself. To the right of the operator, a whiteboard was located, on which the objective checkpoint orders were written. The operator had no direct visual contact with the scenario, even when looking backwards.

2) Navigation Scenarios

While the participant sat in the Teleoperation Station, the UGV was located in the scenario depicted in Fig. 15. This scenario has 18 distinct paths, depending on the order of the checkpoints. The paths were designed so that, depending on the path taken, they can avoid certain objectives.

The scenario was set up in an area measuring 6 m by 8 m. Flexible orange pipes with black strips were used to define

This work is licensed under a Creative Commons Attribution 4.0 License. For more information, see https://creativecommons.org/licenses/by/4.0/

This article has been accepted for publication in IEEE Access. This is the author's version which has not been fully edited and
content may change prior to final publication. Citation information: DOI 10.1109/ACCESS.2026.3749135

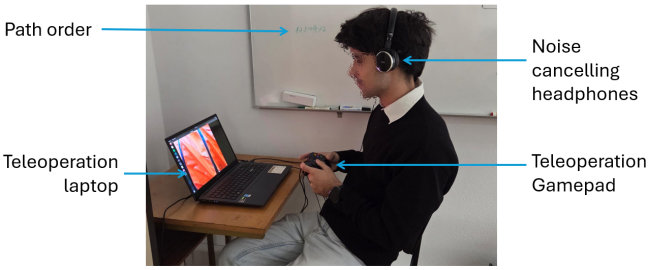


FIGURE 14. Teleoperation station with a participant operating Jackal.

the scenario's boundaries, facilitating its deployment. These pipes ensured that, if the UGV came into contact with the walls, it would remain undamaged while causing minimal impact on the scenario, enabling the continuation of the user study.

The floor was covered with a protective tarpaulin, serving two purposes: safeguarding the underlying surface and eliminating ground references that might help users detect slippage. The tarpaulin was stretched to cover the entire map, preventing major folds or wrinkles that could interfere with the vehicle's movement or provide unintended cues of slippage.



FIGURE 15. User study Scenario with a random checkpoint order.

C. USER STUDY METRICS

In this user study, a within-subject design was adopted, meaning that all participants completed all four conditions. Since the intent was to analyse the parametric metrics using Repeated Measures ANOVA (RM-ANOVA), an evaluation of the minimum size of the participant pool was conducted. The power analysis was done in GPower version 3.1.9.7[5], with an *a priori* power analysis type. The inputs and consequent outputs are shown in Table 5 and Table 6, respectively. As shown in Fig. 16, the results with a power of 95%, a type 1 error of 5%, and an effect size of around 0.5 yield a minimum participant pool of 26 participants. The critical F-value in this case is 2.727, which means anything to the right of this value is considered statistically significant. The red area to the right of the critical F-value depicts the input for Type 1 error (α), which is the probability of incorrectly rejecting the null hypothesis, while the Type 2 error (β) is the blue area to the left, which is the probability of failing to detect a real effect.

The final participant pool comprised 32 participants, resulting in a total margin of 6 participants. To increase the number of data points per disturbance for better statistical analysis and to avoid practice effects, the disturbances were repeated 3 times per trial.

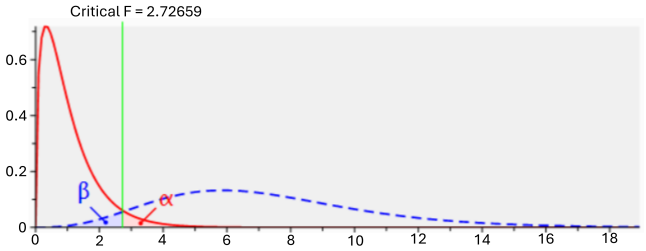


FIGURE 16. Statistical analysis of minimum participant pool for RM-ANOVA.

TABLE 5. GPower analysis inputs

	Input
Effect size f(U)	0.49
α err prob	0.05
Power ($1-\beta$ err prob)	0.95
Number of groups	1
Number of measurements	4
Nonsphericity correction ϵ	1

TABLE 6. GPower analysis outputs

	Output
Noncentrality parameter λ	18.17
Critical F	2.73
Numerator df	3.00
Denominator df	75.00
Total sample size	26
Actual power	0.95

1) Data collected

Table 7 summarizes the direct and indirect measurements collected from participants in the user study, where direct refers to data retrieved directly from participants' interactions, whereas indirect refers to data derived from recordings and therefore does not necessarily involve direct participant interaction. Recordings serve as ground truth for timed disturbances, facilitating analysis of reaction times and alignment with the ROS bags.

2) PHT evaluation metrics mapping to teleoperation SA

To evaluate the effectiveness of the proposed PHT approach, the design and implementation of the user study incorporate targeted performance metrics mapping directly to our two core research questions: RQ1 (SA Level 1 – Perception)

[5]https://www.psychologie.hhu.de/arbeitsgruppen/allgemeine-psychologie-und-arbeitspsychologie/gpower last accessed in 12th of January 2026

This work is licensed under a Creative Commons Attribution 4.0 License. For more information, see https://creativecommons.org/licenses/by/4.0/

This article has been accepted for publication in IEEE Access. This is the author's version which has not been fully edited and
content may change prior to final publication. Citation information: DOI 10.1109/ACCESS.2026.3749135

and RQ2 (SA Level 2 – Comprehension). These metrics, gathered during experimental trials, evaluate how the operator's situational awareness varies under different sensory feedback configurations and are structured across direct and indirect measures, summarized in Table 7. Direct metrics are primarily derived from the real-time 'think-aloud' protocol, alongside post-trial qualitative evaluations and NASA-TLX workload questionnaires.

The direct metrics derived from the real-time 'think-aloud' method. It allows the extraction of the definitive SA evaluation metrics outlined in Table 8. Specifically, RQ1 (Level 1 SA) is quantified by assessing whether an introduced traction loss disturbance is perceived by the user, measuring the response latency from the onset of the event until verbalization (with a 4-second timeout threshold). Conversely, RQ2 (Level 2 SA) focuses on environmental comprehension and reasoning, evaluating whether the operator correctly interprets and verbalizes the specific nature of the event once perceived. Through these metrics, the experimental framework systematically tests our two underlying hypotheses across both levels of SA. Hypothesis I (loss of traction/stuck SA) posits that inducing a PHT visual cue vibration effect will successfully address both RQ1 and RQ2 during a rover loss-of-traction event. Alongside, Hypothesis II (sliding/pushing force SA) addresses both research questions by evaluating whether a PHT sliding visual effect allows operators to reliably perceive (RQ1) and comprehend (RQ2) sliding and pushing forces. Ultimately, the data indexed within Table 8 provide the empirical basis to validate both hypotheses and determine if PHT significantly enhances teleoperation SA.

D. PARTICIPANT DEMOGRAPHICS

A total of 32 unpaid subjects, aged 18 to 29, voluntarily participated in the user study. We guaranteed the anonymity of the participants when collecting data. Each participant was provided with written instructions for the user study procedure and signed an informed consent form. The participants had neither prior experience teleoperating the Jackal nor prior knowledge of the paths to be explored across the several trials. The participants were asked about their gender, age, and whether they had any uncorrected visual impairments, as shown in Appendix A. The following demographic data was collected:

- 75% of participants were men, while 25% were women
- No one had any type of visual impairment

TABLE 7. Summary of direct and indirect metrics gathered through the participants from the User Study.

Category	Metric Description
Direct Measures	(1) **Think-aloud method**: real-time verbalized feedback about system state and environment perception. (2) **Post-trial qualitative evaluation**: questionnaire. (3) **Qualitative evaluation of PHT preference**. (4) **NASA TLX questionnaire** completed on a tablet.
Indirect Measures	(1) **Video recordings** of the teleoperation screen and microphone audio for every trial. (2) **ROS bag recordings** of trial data. (3) **External third-person video recording** of the scenario using a stationary camera.

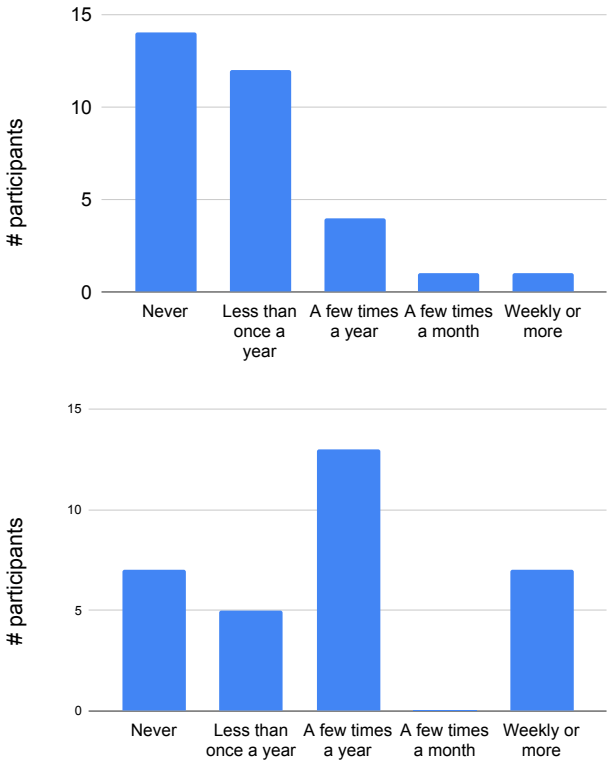


FIGURE 17. Teleoperation use statistics (Top image) and gaming experience (bottom image)

Fig. 17 shows the demographic data regarding the participants' prior experience with teleoperation and video gaming. The top chart indicates that thirty participants had little to no prior experience with teleoperation, with fourteen never having used teleoperation systems and twelve using them less than once a year. Only two participants reported frequent teleoperation (monthly or weekly), suggesting that the study population was largely composed of novice teleoperators. In contrast, the bottom chart shows that participants generally had greater familiarity with video gaming. Twenty participants reported gaming a few times a year (thirteen) or more frequently, with a notable proportion indicating weekly or more frequent gaming (seven). This distribution suggests a higher overall exposure to gaming interfaces compared to teleoperation systems.

E. PROCEDURE

Participants were not briefed on what a PHT is, nor on the effects meaning. The reason for this decision is that if PHT effects are intended to be perceived naturally, they should not be required to be explained.

This work is licensed under a Creative Commons Attribution 4.0 License. For more information, see https://creativecommons.org/licenses/by/4.0/

This article has been accepted for publication in IEEE Access. This is the author's version which has not been fully edited and
content may change prior to final publication. Citation information: DOI 10.1109/ACCESS.2026.3749135

TABLE 8. Evaluation metrics mapping to teleoperation SA research questions

Metric description	Metric start (retrieving)	Metric end (retrieving)	SA Level 1 (perception)	SA Level 2 (comprehension)
Is the introduced disturbance perceived by user?	Stopwatch start (when the disturbance is introduced).	Stopwatch end (when verbalized by user). Time-out after 4s (not noticed by user).	Yes	No
If the event was perceived, what was reported?	Verbalized by the operator.	Not applicable.	No	Yes. Did the operator correctly comprehend the introduced disturbance?

1) Training Session

Each participant completed a training session to familiarize themselves with Jackal's movement input. During this period, the participants had direct visual contact with the robot and were free to control it. The training session was conducted outside the trial scenario to prevent bias during the trials, and the time varied according to how comfortable the participant was with the Rover's operation, but did not exceed 10 minutes.

2) Navigation Challenges

After the training period, each participant completed four trials: one control scenario in which only the Jackal's camera feed was streamed, and three additional trials corresponding to the three different PHTs (Wheels, Peripheral borders, and Particle flow). The trial order, disturbances, and checkpoint orders were randomly selected using a Python script developed specifically to create a complete randomization. This randomization prevents the carry-over effect from trial to trial.

During the trials, the subjects used noise-cancelling headphones with white noise playing in the background to reduce any sound-related cues. White noise has been shown to improve sustained attention and reduce distraction by masking unpredictable environmental sounds [54] [55].

The checkpoint order was written down on a whiteboard near the operator. The operators had to reach the checkpoint according to said order, and, if they did not respect the order, they would have to start over. The participant would have to figure out the order of each checkpoint by themselves. Therefore, it was recommended that they first undergo an exploration phase to see how the scenario and paths were laid out, and then begin the order.

During each trial, participants were asked to report what they thought had happened to the UGV whenever they perceived its motion was disturbed. The movement was disturbed as shown in the Fig. 8, 9 and 10, but they were not explicitly stated to the participants. If the participant completed the path before each disturbance and the corresponding number of repetitions, they would proceed to other randomly selected paths until the trial was over. Every trial was timed using a phone's stopwatch, and whenever a disturbance was not detected after 4 seconds, it was recorded.

3) Post-Trial Questionnaires

After each trial, the participants answered two post-trial questionnaires: (1) a qualitative questionnaire (Appendix B) to assess overall perception of the traction states during that trial, and (2) NASA-TLX[6] to evaluate workload, filled in through a tablet. Once all four trials were complete, the participants were asked about their preference and comments on the PHTs (Appendix C).

VI. USER STUDY RESULTS

A. DISTURBANCE DETECTION

This disturbance detection metric serves as a direct objective behavioral performance indicator, measuring in real-time the responsiveness of operators in identifying dynamic physical disturbances occurrences (such as wheel slippage, sliding, and vehicle stuck states) under each system configuration. For disturbance detection, a Friedman test with descriptive metrics was conducted on the total number of detected disturbances per condition for each disturbance type. This resulted in degrees of freedom of df = 3, reflecting the control condition and PHTs, analyzed separately for each disturbance type, as shown in Table 9. Statistical significance was determined using a threshold of $p < 0.05$. The results indicated that only the "Slide B small" disturbance showed a statistically significant difference between conditions ($\chi^2 = 42.948$, $p < 0.01$). In contrast, the remaining disturbances did not demonstrate significant differences across conditions.

TABLE 9. Friedman test results on disturbance detection

Disturbances	χ^2	p-value
Slide B small	42.948	< 0.01
Slide B big	0.686	0.877
Slide L small	3.873	0.276
Slide L big	1.320	0.724
Slide R small	4.403	0.221
Slide R big	2.063	0.560
Stuck	1.446	0.695

To further understand the significant effect observed for "Slide B small", a post-hoc Wilcoxon signed-rank tests was performed for pairwise comparisons between conditions, as presented in Table 10. The results revealed significantly higher disturbance detection rates for all PHT conditions

[6]https://www.keithv.com/software/nasatlx/nasatlx.html [last accessed 27 Nov 2025]

This work is licensed under a Creative Commons Attribution 4.0 License. For more information, see https://creativecommons.org/licenses/by/4.0/

This article has been accepted for publication in IEEE Access. This is the author's version which has not been fully edited and
content may change prior to final publication. Citation information: DOI 10.1109/ACCESS.2026.3749135

compared to the Control condition, with "Wheels-Control" ($Z = -4.179$, $p < 0.001$), Borders-Control ($Z = -4.592$, $p < 0.001$), and "Flow-Control" ($Z = -3.529$, $p < 0.001$) all showing statistically significant differences. The negative Z-values indicate that disturbance detection performance favored the PHT conditions over the Control condition.

TABLE 10. Wilcoxon's "Slide B small" test results

	Wheels-Control	Borders-Control	Flow-Control
Z	-4.179	-4.592	-3.529
Sig. (2-tailed)	<0.001	<0.001	<0.001
	Borders-Wheels	Flow-Wheels	Flow-Borders
Z	-1.042	-0.879	-1.659
Sig (2-tailed)	0.298	0.379	0.097

No statistically significant differences were found between the PHT conditions themselves. This suggests that, although all PHT conditions improved disturbance detection compared to the Control condition, none of the PHT methods significantly outperformed the others.

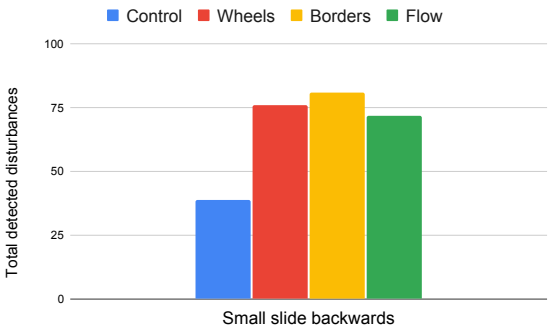


FIGURE 18. Slide B small disturbance detection. Cumulative detected disturbances throughout all participants, per condition

These findings are further supported by Figure 18, which illustrates the substantial increase in the total number of detected "Slide B small" disturbances across participants in the PHT conditions compared to the Control condition.

B. NASA-TLX

A within subject RM-ANOVA was conducted separately for each NASA-TLX dimension. Each dimension was analysed independently, as recommended by Bolton et al. [56], who argue that aggregated workload scores lack meaningful interpretation. The analysis was conducted using a full factorial within-subjects model and included effect-size estimates, observed power, and tests of sphericity. Marginal means were also inspected across conditions.

Mauchly's Test of Sphericity indicated that the assumption of sphericity was met for all dimensions except Physical Demand (χ^2 = 11.722, p = 0.039). Therefore, a Greenhouse–Geisser correction was applied for Physical Demand. All other dimensions satisfied the sphericity assumption (p > 0.05). Table 11 presents Mauchly's test results, and Table 12 (within-subject effects) reports the corresponding repeated-measures ANOVA results, including the Greenhouse–Geisser–corrected results where applicable.

TABLE 11. Mauchly's Test of Sphericity for NASA-TLX Dimensions

Dimension	χ^2	p-value
Mental Demand	5.603	0.347
Physical Demand	11.722	0.039
Temporal Demand	5.662	0.341
Performance	6.522	0.259
Effort	9.430	0.093
Frustration	6.522	0.259

The repeated-measures ANOVA revealed no statistically significant main effects of condition on any NASA-TLX dimension. Mental Demand, Temporal Demand, Effort, and Frustration did not reach significance under the assumption of sphericity (all p > 0.05). Physical Demand, analyzed using Greenhouse–Geisser corrected degrees of freedom, was also not significant, F(2.379, 73.739) = 1.786, p = 0.168.

TABLE 12. Repeated-Measures ANOVA Results for NASA-TLX Dimensions

Dimension	F	df_1	df_2	p-value
Mental Demand	2.375	3	93	0.075
Physical Demand	1.786	2.379	73.739	0.168
Temporal Demand	0.191	3	93	0.902
Performance	2.375	3	93	0.075
Effort	0.577	3	93	0.632
Frustration	2.375	3	93	0.075

Although no statistically significant main effects were observed, the descriptive marginal means suggested a non-significant trend in the Frustration dimension, where Wheels and Flow were rated as less frustrating than Peripheral Borders, with an approximate difference of 10%, as shown in Figure 19.

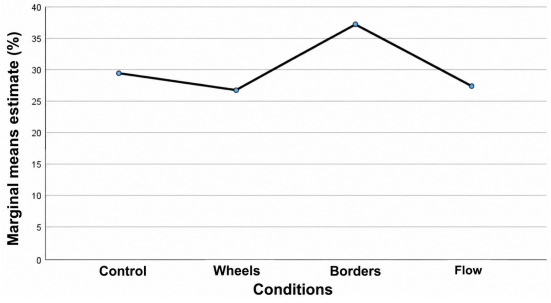


FIGURE 19. Marginal Means for the Frustration Dimension

These findings are further supported by the mode distribution of NASA-TLX responses shown in Figure 20, which summarises the most frequently selected ratings across conditions.

C. POST-TRIAL QUESTIONNAIRE RESULTS

1) Discomfort

Table 13 depicts the Wilcoxon pair-wise results regarding the "Discomfort" metric. The results revealed no statistically

This work is licensed under a Creative Commons Attribution 4.0 License. For more information, see https://creativecommons.org/licenses/by/4.0/

This article has been accepted for publication in IEEE Access. This is the author's version which has not been fully edited and
content may change prior to final publication. Citation information: DOI 10.1109/ACCESS.2026.3749135

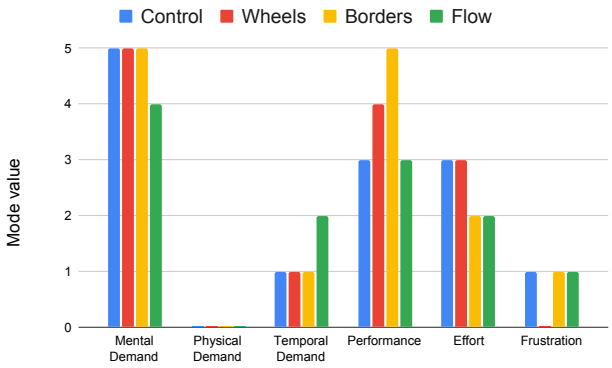


FIGURE 20. Mode of NASA-TLX Tally Responses

significant differences in perceived discomfort between any pair of conditions. In particular, the "Flow-Control" comparison produced a Z-value of 0.000 and a significance value of 1.000, indicating no systematic difference between the two paired conditions, being consistent with the null hypothesis. It is therefore demonstrated that there was no additional discomfort when adding the effects that compose the PHTs complementing the results obtained with the NASA-TLX.

TABLE 13. Wilcoxon's Discomfort test results

	Wheels-Control	Borders-Control	Flow-Control
Z	-0.333	-1.311	0.000
Sig. (2-tailed)	0.739	0.190	1.000
	Borders-Wheels	Flow-Wheels	Flow-Borders
Z	-0.973	-0.250	-1.098
Sig. (2-tailed)	0.331	0.803	0.272

2) How clear were the different effects displayed throughout the trial

Table 14 shows the results regarding perceived clarity of the different effects displayed throughout the trial indicate statistically significant differences between most condition pairs, with the exception of the Flow–Control comparison ($Z = 0.000, p = 1.000$), which showed no evidence of a systematic difference and is fully consistent with the null hypothesis. Overall, the results suggest that participants perceived the Wheels ($Z = -4.140, p < 0.001$) and Peripheral borders ($Z = -3.549, p < 0.001$) conditions as providing clearer representations of the different effects compared to both the Control and Flow conditions. In particular, Flow did not differ significantly from Control, indicating that participants did not perceive an improvement in clarity when using this condition.

These findings are consistent with the mode results shown in Figure 21, where Wheels and Peripheral borders conditions exhibit higher perceived clarity ratings, while Flow and Control show comparatively lower and more similar ratings. This pattern may suggest that, on Flow, either the effects were not sufficiently distinguishable for participants or that the effects were too subtle for participants to detect any meaningful differences between them.

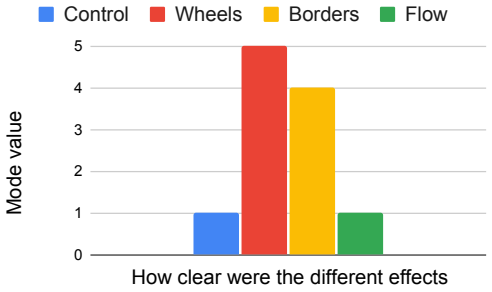


FIGURE 21. Mode of "How clear were the different effects displayed throughout the trial" [1-Not clear; 5-Very clear]

TABLE 14. Wilcoxon's "How clear were the different effects displayed throughout the trial" test results

	Wheels-Control	Borders-Control	Flow-Control
Z	-4.140	-3.549	0.000
Sig. (2-tailed)	<0.001	<0.001	1.000
	Borders-Wheels	Flow-Wheels	Flow-Borders
Z	-2.295	-4.140	-3.549
Sig. (2-tailed)	0.022	<0.001	<0.001

3) How clear was the interface as a whole

Table 15 demonstrates that there are statistically significant differences between all PHT conditions and the Control condition. These findings indicate that all tested PHT conditions were perceived as significantly clearer than the Control condition. In contrast, no statistically significant differences were observed between any of the PHT conditions themselves. The general clarity of the effects seems to align with the perception that adding the PHTs adds meaning to the disturbances that are occurring on the UGV and that changes are more perceptible with PHTs when compared to the control condition.

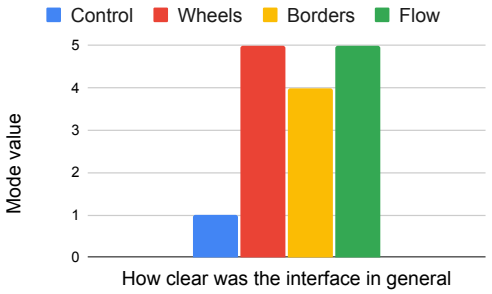


FIGURE 22. Mode of "How clear was the interface in general" [1-Not clear; 5-Very clear]

4) Stuck detection difficulty

Table 16 shows that results indicate statistically significant differences between the "Borders–Control" ($Z = -2.872$,

This work is licensed under a Creative Commons Attribution 4.0 License. For more information, see https://creativecommons.org/licenses/by/4.0/

This article has been accepted for publication in IEEE Access. This is the author's version which has not been fully edited and content may change prior to final publication. Citation information: DOI 10.1109/ACCESS.2026.3749135

TABLE 15. Wilcoxon's "How clear was the interface in general" test results

	Wheels-Control	Borders-Control	Flow-Control
Z	-3.940	-3.832	-4.077
Sig. (2-tailed)	<0.001	<0.001	<0.001
	Borders-Wheels	Flow-Wheels	Flow-Borders
Z	-0.661	-0.798	-1.570
Sig. (2-tailed)	0.509	0.425	0.116

$p = 0.004$) and "Flow–Control" ($Z = -2.952$, $p = 0.003$) comparisons, suggesting that both PHT conditions improved participants' ability to detect the stuck disturbance relative to the Control condition. In contrast, the "Wheels–Control" comparison did not reach statistical significance ($Z = -1.443$, $p = 0.149$), indicating no clear difference between these conditions. No statistically significant differences were found between any of the PHT conditions themselves.

Overall, these findings suggest that the peripheral borders and Particles flow PHT conditions provide a measurable improvement in stuck detection compared to the Control condition, whereas the Wheels condition does not show a statistically reliable improvement. This may indicate that the "Stuck" feedback implemented in Wheels is less effective or less perceptible to participants, despite the overall disturbance detection results for this condition not showing significant anomalies.

TABLE 16. Wilcoxon's Stuck Difficulty test results

	Wheels-Control	Borders-Control	Flow-Control
Z	-1.443	-2.872	-2.952
Sig. (2-tailed)	0.149	0.004	0.003
	Borders-Wheels	Flow-Wheels	Flow-Borders
Z	-1.047	-1.485	-0.842
Sig. (2-tailed)	0.295	0.138	0.400

5) Slide detection difficulty

The results shown on Table 17 regarding the perceived difficulty of detecting sliding disturbances indicate a statistically significant difference only for the "Flow–Control" comparison ($Z = -2.652$, $p = 0.008$), suggesting that participants were significantly better able to perceive sliding disturbances under the Flow condition compared to the Control condition. In contrast, the "Wheels–Control" ($Z = -1.392$, $p = 0.164$) and "Borders–Control" ($Z = -1.223$, $p = 0.221$) comparisons did not reach statistical significance, indicating no reliable difference between these conditions and the Control condition. Additionally, no statistically significant differences were observed between any of the PHT conditions themselves.

This suggests that participants perceived the sliding disturbances more noticeably with "Flow" compared to the control condition, indicating that it was considered more perceptible than the other conditions.

TABLE 17. Wilcoxon's Slide Difficulty test results

	Wheels-Control	Borders-Control	Flow-Control
Z	-1.392	-1.223	-2.652
Sig. (2-tailed)	0.164	0.221	0.008
	Borders-Wheels	Flow-Wheels	Flow-Borders
Z	-0.566	-0.647	-1.310
Sig. (2-tailed)	0.572	0.518	0.190

6) Immersiveness

For perceived immersiveness the results shown on Table 18 statistically significant differences for the "Wheels–Control" ($Z = -2.053$, $p = 0.040$) and "Borders–Control" ($Z = -2.235$, $p = 0.025$) comparisons, indicating that both PHT conditions were perceived as more immersive than the Control condition. The "Flow–Control" comparison approached significance ($Z = -1.890$, $p = 0.059$), suggesting a similar trend but without sufficient evidence to confirm a statistically reliable difference. No statistically significant differences were found between any of the PHT conditions themselves, indicating that all PHT implementations produced comparable levels of immersiveness.

Overall, although Figure 23 does not show strong visual separation between conditions, the Wilcoxon signed-rank tests suggest a modest increase in perceived immersiveness for the Wheels and Borders conditions relative to the Control condition, with a consistent positive trend also observed for the Flow condition.

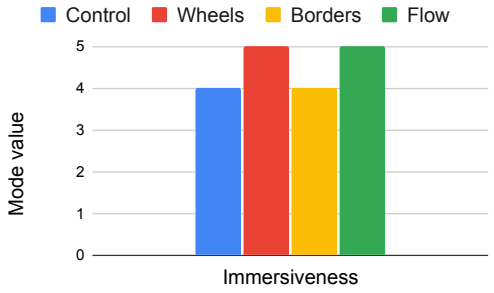


FIGURE 23. Mode of immersiveness [1-Not immersive; 5-Very immersive]

TABLE 18. Wilcoxon's Immersiveness test results

	Wheels-Control	Borders-Control	Flow-Control
Z	-2.053	-2.235	-1.890
Sig. (2-tailed)	0.040	0.025	0.059
	Borders-Wheels	Flow-Wheels	Flow-Borders
Z	-0.632	-1.026	-1.000
Sig (2-tailed)	0.527	0.305	0.317

7) Usefulness

Table 19 demonstrates statistically significant differences between all PHT conditions and the Control condition. These findings suggest that participants consistently perceived all

This work is licensed under a Creative Commons Attribution 4.0 License. For more information, see https://creativecommons.org/licenses/by/4.0/

This article has been accepted for publication in IEEE Access. This is the author's version which has not been fully edited and
content may change prior to final publication. Citation information: DOI 10.1109/ACCESS.2026.3749135

PHT implementations as more useful than the Control condition. In addition, a statistically significant difference was observed between the "Flow–Borders" pair ($Z = -2.035$, $p = 0.042$), indicating that Flow was perceived as more useful than Borders. This is in accordance to what was hypothesized, since the users would naturally realize that this type of PHTs added information to what was happening to the UGV, when compared to the Control condition.

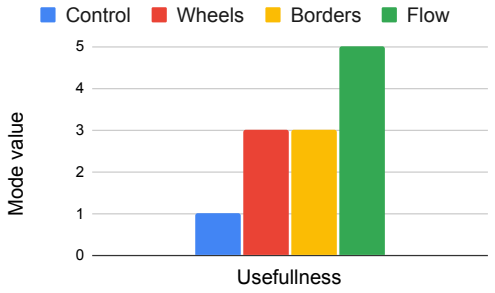


FIGURE 24. Mode of usefulness [1-Not useful; 5-Very useful]

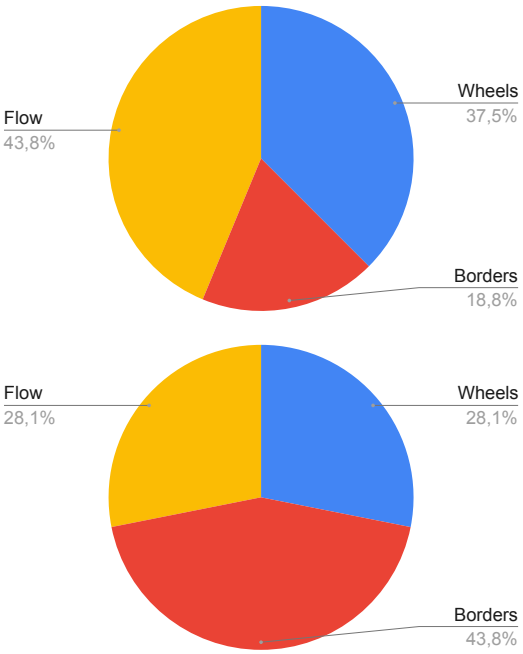


FIGURE 25. Participant's distribution regarding their favorite PHT (top) and the one they disliked the most (bottom)

TABLE 19. Wilcoxon's Usefulness test results

	Wheels-Control	Borders-Control	Flow-Control
Z	-3.907	-3.803	-4.181
Sig. (2-tailed)	<0.001	<0.001	<0.001
	Borders-Wheels	Flow-Wheels	Flow-Borders
Z	-0.652	-1.108	-2.035
Sig. (2-tailed)	0.514	0.268	0.042

D. PHT PREFERENCE RESULTS

Fig. 25 shows the pie charts summarizing the responses to the post-trial questionnaire (Appendix C) from the 32 participants, indicating their preferred PHT and the one they disliked the most, respectively. The results indicate no clear consensus on the most preferred PHT, with Flow and Wheels yielding similar results. In contrast, Peripheral Borders show a supposed depreciation relative to the others.

E. OBJECTIVE VS. SUBJECTIVE EVALUATION SUMMARY

To complement the post-trial subjective evaluations (e.g., NASA-TLX, clarity, usefulness, and immersiveness), our evaluation framework specifically incorporates real-time disturbance detection performance (Section VI-A) as an objective behavioural indicator. The objective metrics demonstrate a statistically significant enhancement in operators' ability to identify subtle locomotion disturbances ("Slide B small", $p < 0.01$) across all PHT conditions relative to the Control condition. This objective performance gain aligns directly with the subjective findings, confirming that the perceived visual clarity and usefulness translate directly into measurable improvements in operator situation awareness during teleoperation.

VII. DISCUSSION

A. DISTURBANCE DETECTION

The results revealed that the only disturbance with statistically significant differences across conditions was "Slide B small". The post-hoc Wilcoxon tests indicated that both Peripheral Borders and Flow PHTs yielded significantly higher detection rates than the Control condition, whereas there were no significant differences between the PHTs. This indicates that PHTs effectively improve users' ability to perceive subtle disturbances, particularly for small backwards sliding events.

B. WORKLOAD (NASA-TLX)

Analysis of the NASA-TLX data showed that none of the workload dimensions were significantly affected by the addition of PHTs. The marginal means suggested a slight trend in reduced frustration for Wheels and Flow PHTs compared to Peripheral Borders, but this difference was not statistically significant when looking at the data gathered in Table 11. Overall, these findings demonstrate that the integration of PHTs maintained the operator's workload at a sustainable level.

C. POST-TRIAL QUESTIONNAIRE

Participants reported greater clarity and detectability of disturbances when using PHTs than in Control, particularly in the "How clear was the interface as a whole" and "Slide detection difficulty" questions. Immersiveness and perceived usefulness were also rated higher with PHTs, with Flow appearing to be slightly preferred for usefulness. In alignment with the NASA-TLX findings, no significant differences in

This work is licensed under a Creative Commons Attribution 4.0 License. For more information, see https://creativecommons.org/licenses/by/4.0/

This article has been accepted for publication in IEEE Access. This is the author's version which has not been fully edited and
content may change prior to final publication. Citation information: DOI 10.1109/ACCESS.2026.3749135

physical discomfort were observed across conditions. The lack of increased discomfort, coupled with improved subtle slide detection rates, suggests that PHTs are a promising, non-intrusive solution for enhancing Situation Awareness (SA) in traction-related tasks.

D. PARTICIPANT'S FEEDBACK AND PREFERENCES

A limitation of the present user study is the use of a convenience sample comprising university students rather than professional rover operators. While testing with non-experts was essential for establishing a baseline evaluation of how intuitive PHT visual cues are without prior domain training. For novice operators, dynamic visual cues serve as explicit cognitive support to aid disturbance recognition. Future evaluations could compare expert and novice cohorts to investigate whether PHT visual cues remain beneficial. On Appendix D, Table 20, Table 21 and Table 22 show some selected comments regarding each PHT. These comments are either directly cited, or translated from Portuguese to English. Participant comments reflected diverse experiences and preferences. Wheels were appreciated for their intuitiveness and constant visibility, but occasionally perceived as occupying too much screen space. Periheral Borders were useful for understanding directionality, but could be confusing or overwhelming for some users. Flow provided a perceptually subtle but responsive cue, though some participants found it distracting or unclear. There was no unanimous preference among participants, with Periheral Borders the least favored. In summary, the feedback shows that each PHT approach offers distinct advantages and trade-offs, catering to different user preferences and perceptual tendencies.

E. PHT AND FORCE FEEDBACK SYSTEM CONSIDERATIONS

From literature, force feedback plays an important role in teleoperation systems, providing haptic cues that enhance collision awareness and interaction force regulation. Instead, our PHT system focuses on PHT as a visual-perceptual induced effect to convey terrain-vehicle interactions and dynamic disturbances. PHT bypasses the haptic devices hardware-level and stability control challenges, by modulating visual feedback. Nevertheless, integrating active haptic devices remains a valuable option. Future iterations of this work could explore combining PHT with force-feedback interfaces, where PHT effects could be integrated (by modulating visual feedback) as complementary to a force feedback device. This way, the authors foresee integrating active haptic devices with PHT as a valuable possible future direction.

F. OVERALL DISCUSSION

Results across performance metrics, workload, and qualitative feedback indicate that PHTs enhanced operator awareness of subtle traction-related events without increasing cognitive demand. All PHT conditions outperformed the Control in disturbance detection, for subtle events like minor backward slides. While it could be argued that focusing on subtle disturbances minimizes the impact, we contend that this reinforces the relevance of PHT. SA breakdowns in teleoperation often stem from low-salience discrepancies rather than catastrophic failures. Operators typically detect large-scale failures unaided but struggle to identify early indicators such as partial slip or reduced efficiency [2], [22]. By surfacing these early cues, PHTs facilitate corrective action before unsafe states occur.

The qualitative trade-off between saliency and distraction accounts for the absence of a single "optimal" PHT design. While *Wheels* utilized familiar metaphors, *Particle Flow* was more informative but potentially distracting. These findings align with Endsley's level SA model, addressing the two RQs:

- **RQ1- SA Level 1 (Perception):** Compared to the control condition, PHTs conditions improved the detection of subtle sliding traction losses perceptually salient (otherwise invisible vehicle states).
- **RQ2 - SA Level 2 (Comprehension):** Participants correctly associated PHT cues with physical phenomena (e.g., sliding direction), indicating successful information mapping across all designs.

NASA-TLX results confirmed that PHTs did not increase perceived mental or temporal demand. The *Particle Flow* design exhibited a balanced profile with low frustration, whereas *Peripheral Borders* reduced workload but occasionally led to lower perceived performance. This suggests that minimizing cognitive demand does not always equate to increased operator confidence. Furthermore, post-trial feedback highlighted that dynamic cues (e.g., *Particle Flow*) seem to better convey gradual disturbances compared to static metaphors.

VIII. CONCLUSION

This paper proposes and evaluates a novel PHT approach for enhancing SA during rover teleoperation, specifically regarding traction loss and sliding. By comparing three PHT designs (*Wheels, Peripheral Borders, and Particle Flow*) against a visual-only control condition, we demonstrated that PHTs improve the detection of subtle slide disturbances without increasing operator workload.

Key findings indicate that PHTs are most effective at surfacing low-intensity events, such as backward slides, which are inherently difficult to perceive from monocular camera feeds alone. PHTs partially provided the critical perceptual SA for early-stage degradation. NASA-TLX results confirmed that this additional information layer does not impose significant cognitive or physical burdens. Notably, *Particle Flow* emerged as a balanced design, offering high clarity and low frustration, while *Peripheral Borders* minimized demand but occasionally reduced user confidence.

Qualitative feedback highlighted a fundamental trade-off between cue saliency and distraction. The lack of a single optimal design across all metrics, coupled with strong inter-individual preferences, suggests that the PHT design space is flexible. Future teleoperation interfaces should favor adaptable or customizable PHT configurations to accommodate diverse operator strategies and experience levels.

This work is licensed under a Creative Commons Attribution 4.0 License. For more information, see https://creativecommons.org/licenses/by/4.0/

This article has been accepted for publication in IEEE Access. This is the author's version which has not been fully edited and
content may change prior to final publication. Citation information: DOI 10.1109/ACCESS.2026.3749135

In summary, PHTs offer a promising modality for enhancing SA in UGV teleoperation by externalizing subtle and ambiguous vehicle states. Future work will investigate the longitudinal impact of PHTs on objective navigation effectiveness and recovery times, and also focus on user-centered customization to balance cue saliency with individual attention strategies.

APPENDIX A
DEMOGRAPHIC QUESTIONNAIRE

- Gender
  - Man
  - Woman
  - Others
  - Rather not say
- Age
  - 18–29
  - 30–44
  - 45–59
  - 60+
- Do you have any visual impairment (that is not corrected)?
  - Yes/No
  - If you do, what is/are it/they? _____
- How often do you use teleoperation (drones, teleoperated cars, etc.)?
  - Never
  - Less than once a year
  - A few times a year
  - A few times a month
  - Weekly or more
- How often do you play video games with a controller?
  - Never
  - Less than once a year
  - A few times a year
  - Weekly or more

APPENDIX B
POST-TRIAL QUALITATIVE QUESTIONNAIRE

- Were you distracted at a certain point during the trial?
  - Yes/No
- How difficult was it to understand that the robot was stuck?
  - Scale: [1 – Very easy, 5– Very difficult]
- How difficult was it to understand that the robot was sliding?
  - Scale: [1 – Very easy, 5– Very difficult]
- Level of discomfort during the operation? This means being uncomfortable physically or mentally when operating the UGV.
  - Scale: [1 – No Discomfort, 5– Very Discomforting]
- How clear were the different effects displayed throughout the trial?
  - Scale: [1 – Not Clear, 5– Very Clear]
- How clear were the effects?
  - Scale: [1- Not Clear, 5- Very Clear]
- How immersive was the experience while using the interface? Immersive means being engaged in the task at hand through the interaction with the interface.
  - Scale: [1 – Not immersive, 5– Extremely immersive]
- How useful were the effects displayed whenever a disturbance occurred for the UGV teleoperation?
  - Scale: [1 – Not useful, 5– Very useful]

APPENDIX C
PHT PREFERENCE

- What PHT did you prefer the most?
  - Particles
  - Wheels
  - Peripheral borders
- Can you justify your previous choice?
  - _____
- What PHT did you like the least?
  - Particles
  - Wheels
  - Peripheral borders
- Can you justify your previous choice?
  - _____
- What are the positive aspects of:
  - Particles
  - _____
  - Wheels
  - _____
  - Peripheral borders
  - _____
- What are the negative aspects of:
  - Particles
  - _____
  - Wheels
  - _____
  - Peripheral borders
  - _____

APPENDIX D
PARTICIPANT'S COMMENTS

The participants comments for each PHT condition are summarized in Table 20, 21, , and 22.

REFERENCES

[1] Bolton, Matthew L., and Ellen J. Bass. "Comparing perceptual judgment and subjective measures of spatial awareness." Situational Awareness. Routledge, 2017. 211-222.
[2] Endsley, Mica R., and Daniel J. Garland, eds. Situation awareness analysis and measurement. CRC press, 2000.
[3] Gao, H., Guo, J., Ding, L., Li, N., Liu, Z., Liu, G., & Deng, Z. (2013). "Longitudinal skid model for wheels of planetary exploration rovers based on terramechanics". Journal of Terramechanics, 50(5-6), 327-343.

This work is licensed under a Creative Commons Attribution 4.0 License. For more information, see https://creativecommons.org/licenses/by/4.0/

This article has been accepted for publication in IEEE Access. This is the author's version which has not been fully edited and
content may change prior to final publication. Citation information: DOI 10.1109/ACCESS.2026.3749135

TABLE 20. Participant's comments regarding Wheels

Comment type	Quotes
Positive Comments	**Participant 3**: ''The wheels are always visible through the run, therefore any changes to it are very easily noticeable. Moreover, they represent common visual elements that we see everyday, making them very intuitive.'' **Participant 6**: ''As they were always on the interface, they worked as a good reference.''
Negative Comments	**Participant 19**: ''Maybe it was because it is my first trial, but I felt that they occupied the screen and did not do their job properly'' **Participant 28**: ''They were clearly visible, but I did not understand well what they were doing and I took way too long to find out.''

TABLE 21. Participant's comments regarding Periheral Borders

Comment type	Quotes
Positive Comments	**Participant 1**: ''Overall the most useful one I believe because you can clearly understand the different events and you can also understand the directions in which events happened, like sliding.'' **Participant 26**: ''The easiest one to keep immersed in driving while being informed of the disturbance.''
Negative Comments	**Participant 3**: ''It was hard to distinguish periheral borders as a visual indicator or just display issues when a slid or lag happens.'' **Participant 18**: ''There was too much happening, such that there some occurrences that felt were very similar in the PHT response.''

TABLE 22. Participant's comments regarding Flow

Comment type	Quotes
Positive Comments	**Participant 17**: ''Gave a light feel to the interface and it was pretty perceptible the type of disturbances'' **Participant 18**: ''The bubbles felt more responsive to the disturbances and where easier to understand.''
Negative Comments	**Participant 12**: ''I did not understand their purpose.'' **Participant 16**: ''It was very distracting''

[4] Jia, Zhenzhong, William Smith, and Huei Peng. "Terramechanics-based wheel–terrain interaction model and its applications to off-road wheeled mobile robots." Robotica 30.3 (2012): 491-503.

[5] Nielsen, Curtis W., Michael A. Goodrich, and Robert W. Ricks. "Ecological interfaces for improving mobile robot teleoperation." IEEE Transactions on Robotics 23.5 (2007): 927-941.

[6] Khurshid, Rebecca P., et al. "Effects of grip-force, contact, and acceleration feedback on a teleoperated pick-and-place task." IEEE transactions on haptics 10.1 (2016): 40-53.

[7] Giudici, Gabriele, et al. "Haptic Stiffness Perception Using Hand Exoskeletons in Tactile Robotic Telemanipulation." IEEE Robotics and Automation Letters (2025).

[8] Ye, Yang, et al. "Brain functional connectivity under teleoperation latency: a fNIRS study." Frontiers in Neuroscience 18 (2024): 1416719.

[9] Corujeira, Jéssica, José Luís Silva, and Rodrigo Ventura. "Effects of haptic feedback in dual-task teleoperation of a mobile robot." IFIP Conference on Human-Computer Interaction. Cham: Springer International Publishing, 2017.

[10] Leonardis, Daniele, et al. "Hand teleoperation with combined kinaesthetic and tactile feedback: A full upper limb exoskeleton interface enhanced by tactile linear actuators." Robotics 13.8 (2024): 119.

[11] Khurshid, Rebecca P., et al. "Effects of grip-force, contact, and acceleration feedback on a teleoperated pick-and-place task." IEEE transactions on haptics 10.1 (2016): 40-53.

[12] Pusch, Andreas, Olivier Martin, and Sabine Coquillart. "Hemp-hand-displacement-based pseudo-haptics: a study of a force field application." 2008 IEEE Symposium on 3D User Interfaces. IEEE, 2008.

[13] Lim, Woan Ning, et al. "A systematic review of weight perception in virtual reality: techniques, challenges, and road ahead." IEEE Access 9 (2021): 163253-163283.

[14] Kang, HyeongYeop, Geonsun Lee, and JungHyun Han. "Visual manipulation for underwater drag force perception in immersive virtual environments." 2019 IEEE Conference on Virtual Reality and 3D User Interfaces (VR). IEEE, 2019.

[15] Lécuyer, Anatole, et al. "Pseudo-haptic feedback: Can isometric input devices simulate force feedback?." Proceedings IEEE Virtual Reality 2000 (Cat. No. 00CB37048). IEEE, 2000.

[16] Hirao, Yutaro, et al. "Revisiting walking-in-place by introducing step-height control, elastic input, and pseudo-haptic feedback." IEEE Transactions on Visualization and Computer Graphics 30.7 (2022): 3210-3223.

[17] A. Lecuyer, "Playing with Senses in VR: Alternate Perceptions Combining Vision and Touch" in IEEE Computer Graphics and Applications, vol. 37, no. 01, pp. 20-26, Jan.-Feb. 2017, doi: 10.1109/MCG.2017.14.

[18] Kawabe, Takahiro. "Mid-air action contributes to pseudo-haptic stiffness effects." IEEE Transactions on Haptics 13.1 (2019): 18-24.

[19] Rui Xavier, José Luís Silva, and Rodrigo Ventura. 2024. Pseudo-haptics Interfaces for Robotic Teleoperation. In Companion of the 2024 ACM/IEEE International Conference on Human-Robot Interaction (HRI '24). Association for Computing Machinery, New York, NY, USA, 1139–1142, doi: 10.1145/3610978.3640704

[20] Moniruzzaman, MD & Rassau, Alexander & Chai, Douglas & Islam, Syed. (2021). Teleoperation methods and enhancement techniques for mobile robots: A comprehensive survey. Robotics and Autonomous Systems. 150. 103973. 10.1016/j.robot.2021.103973.

[21] J. Scholtz, J. Young, J. L. Drury and H. A. Yanco, "Evaluation of human-robot interaction awareness in search and rescue," IEEE International Conference on Robotics and Automation, 2004. Proceedings. ICRA '04. 2004, New Orleans, LA, USA, 2004, pp. 2327-2332 Vol.3, doi: 10.1109/ROBOT.2004.1307409.

[22] R. Luz, J. Corujeira, J. L. Silva and R. Ventura, "Traction Awareness Through Haptic Feedback for the Teleoperation of UGVs," 2018 27th IEEE International Symposium on Robot and Human Interactive Communication (RO-MAN), Nanjing, China, 2018, pp. 313-319, doi: 10.1109/ROMAN.2018.8525740.

[23] Pacchierotti, Claudio, et al. "Wearable haptic systems for the fingertip and the hand: taxonomy, review, and perspectives." IEEE transactions on haptics 10.4 (2017): 580-600.

[24] Rodríguez-Sedano, Francisco J., et al. "Measuring the impact of haptic feedback in collaborative robotic scenarios." Universal Access in the Information Society 23.3 (2024): 1031-1049.

[25] Lin, Yinjie, Zheng Chen, and Bin Yao. "Unified motion/force/impedance control for manipulators in unknown contact environments based on robust model-reaching approach." IEEE/ASME Transactions on Mechatronics 26.4 (2021): 1905-1913.

[26] Han, L., Mao, J., Cao, P., Gan, Y., & Li, S. (2021). "Toward sensorless interaction force estimation for industrial robots using high-order finite-time observers". IEEE Transactions on Industrial Electronics, 69(7), 7275-7284.

[27] Huang, F., Li, W., Wang, Y., Mei, D., & Chen, Z. (2024). A shared control framework with constrained optimization and guiding force feedback for teleoperation of underwater electric manipulator. IEEE Journal of Oceanic Engineering, 50(2), 1030-1044.

[28] Van den Berg, Alex, et al. "Augmenting visual feedback with visualized interaction forces in haptic-assisted virtual-reality teleoperation." Frontiers in Robotics and AI 11 (2024): 1427095.

[29] Fink, Paul DS, et al. "Expanded situational awareness without vision: a novel haptic interface for use in fully autonomous vehicles." Proceedings of the 2023 ACM/IEEE International Conference on Human-Robot Interaction. 2023.

[30] R. Luz, J. Corujeira, J. L. Silva, and R. Ventura. Traction awareness through haptic feedback for the teleoperation of ugvs. In 2018 27th IEEE International Symposium on Robot and Human Interactive Communication (RO-MAN), pages 313–319, 2018. doi: 10.1109/ROMAN.2018.8525740.

[31] Xia, Pengxiang & Xu, Fang & Song, Zhuoyuan & Li, Shuai & Du, Jing. (2023). Sensory augmentation for subsea robot teleoperation. Computers in Industry. 145. 103836. 10.1016/j.compind.2022.103836.

[32] D. Zhang, G. Yang and R. P. Khurshid, "Haptic Teleoperation of UAVs Through Control Barrier Functions," in IEEE Transactions

This work is licensed under a Creative Commons Attribution 4.0 License. For more information, see https://creativecommons.org/licenses/by/4.0/

This article has been accepted for publication in IEEE Access. This is the author's version which has not been fully edited and
content may change prior to final publication. Citation information: DOI 10.1109/ACCESS.2026.3749135

on Haptics, vol. 13, no. 1, pp. 109-115, 1 Jan.-March 2020, doi: 10.1109/TOH.2020.2966485.

[33] V. Ramachandran, M. Macchini and D. Floreano, "Arm-Wrist Haptic Sleeve for Drone Teleoperation," in IEEE Robotics and Automation Letters, vol. 7, no. 4, pp. 12054-12061, Oct. 2022, doi: 10.1109/LRA.2021.3122107.

[34] Vimal VP, Panic AS, Lackner JR, DiZio P. Vibrotactile feedback as a countermeasure for spatial disorientation. Front Physiol. 2023 Nov 3;14:1249962. doi: 10.3389/fphys.2023.1249962. PMID: 38028769; PMCID: PMC10657135.

[35] Murphy, Robin R. "Case studies of applying Gibson's ecological approach to mobile robots." IEEE Transactions on Systems, Man, and Cybernetics-Part A: Systems and Humans 29.1 (2002): 105-111.

[36] Norman, Donald A. "Affordance, conventions, and design." Interactions 6.3 (1999): 38-43.

[37] Misztal, Sebastian, Guillermo Carbonell, and Jonas Schild. "Experiencing age-related movement impairment through visual delegation in VR can substitute haptic impairments of an age simulation suit." 2022 IEEE 10th International Conference on Serious Games and Applications for Health (SeGAH). IEEE, 2022.

[38] R. Xavier, J. L. Silva, R. Ventura and J. A. P. Jorge, "Pseudo-Haptics Survey: Human-Computer Interaction in Extended Reality and Teleoperation," in IEEE Access, vol. 12, pp. 80442-80467, 2024, doi: 10.1109/ACCESS.2024.3409449.

[39] James, Kim. "The ecological approach to visual perception." (1981): 86-87.

[40] Vicente, K. J., & Rasmussen, J. (1990). The Ecology of Human-Machine Systems II: Mediating "Direct Perception" in Complex Work Domains. Ecological Psychology, 2(3), 207–249.

[41] Vicente, Kim J. "Ecological interface design: Progress and challenges." Human factors 44.1 (2002): 62-78.

[42] Rasmussen, J. (1974). The human data processor as a system component. Bits and pieces of a model. Risø National Laboratory. Risø-M No. 1722

[43] Li, Weihua, et al. "Teleoperation of wheeled mobile robots subject to longitudinal slipping and lateral sliding by time-domain passivity controller." Mechatronics 81 (2022): 102705.

[44] Gaël van der Lee, Anatole Lécuyer, Maxence Naud, Reinhold Scherer, François Cabestaing, et al.. Towards the Automatic Detection of Vection in Virtual Reality Using EEG. 2025. ffhal-05304254

[45] Riecke BE, Feuereissen D, Rieser JJ, McNamara TP. More than a cool illusion? Functional significance of self-motion illusion (circular vection) for perspective switches. Front Psychol. 2015 Aug 10;6:1174. doi: 10.3389/fpsyg.2015.01174. PMID: 26321989; PMCID: PMC4531211.

[46] Lungaro, Pietro, et al. "Gaze-aware streaming solutions for the next generation of mobile VR experiences." IEEE transactions on visualization and computer graphics 24.4 (2018): 1535-1544.

[47] Strasburger, Hans, Ingo Rentschler, and Martin Jüttner. "Peripheral vision and pattern recognition: A review." Journal of vision 11.5 (2011): 13-13.

[48] Lécuyer, Anatole. "Simulating haptic feedback using vision: A survey of research and applications of pseudo-haptic feedback." Presence: Teleoperators and Virtual Environments 18.1 (2009): 39-53.

[49] Ferreira, Miguel, Luís Moreira, and António Lopes. "Differential drive kinematics and odometry for a mobile robot using TwinCAT." Electronic Research Archive 31.4 (2023).

[50] Thrun, Sebastian. "Probabilistic robotics." Communications of the ACM 45.3 (2002): 52-57.

[51] Siegwart, Roland, Illah Reza Nourbakhsh, and Davide Scaramuzza. Introduction to autonomous mobile robots. MIT press, 2011.

[52] Kelly, Alonzo. Mobile robotics: mathematics, models, and methods. Cambridge University Press, 2013.

[53] Deodato, Michele, and David Melcher. "Continuous temporal integration in the human visual system." Journal of vision 24.13 (2024): 5-5.

[54] G. Söderlund, S. Sikström, and P. Smart. Listen to the noise: noise is beneficial for cognitive performance in inattentive children. Behavioral and Brain Functions, 6(55), 2010. doi: 10.1186/1744-9081-6-55.

[55] M. Awada, Y. A. Al-Omari, F. Ahmed, and et al. Optimal white noise levels for cognitive performance, creativity, and stress: A controlled office experiment. Scientific Reports, 12:15025, 2022. doi: 10.1038/s41598-022-18862-w.

[56] M. L. Bolton, E. Biltekoff, and L. Humphrey. The mathematical meaninglessness of the nasa taskload index: A level of measurement analysis. IEEE Transactions on Human-Machine Systems, 53(3):590–599, 2023. doi: 10.1109/THMS.2023.3263482.

[57] A. Meschtscherjakov, S. Strumegger, and S. Tr¨ osterer. Bubble margin: Motion sickness prevention while reading on smartphones in vehicles. In D. Lamas, F. Loizides, L. Nacke, H. Petrie, M. Winckler, and P. Zaphiris, editors, Human-Computer Interaction– INTERACT 2019, pages 660–677, Cham, 2019. Springer International Publishing. ISBN 978-3-030-29384-0.

RUI XAVIER is a PhD candidate of the doctoral Programme in Electrical and Computer Engineering (PDEEC), Instituto Superior Tecnico (IST), Universidade de Lisboa, with a degree in Electronic Systems and Computers Engineering also from IST. My professional experience spans telecommunications, medical equipment, and electronics. Current main research interests are related to computer vision, machine learning, human-computer interaction, and human-robot interaction, aiming to contribute to multimodal immersive teleoperation and data visualization interfaces for improved awareness in ocean and space robotic exploration

JOÃO BATISTA is a MSc student in Electrical and Computer Engineering at Instituto Superior Técnico (IST), Universidade de Lisboa. His research interests are related to computer vision, machine learning, autonomous vehicles and human-robot interaction, with experience in academic projects related to autonomous systems, more specifically autonomous cars. He is currently working on robotic cameras and computer vision.

JESSICA CORUJEIRA holds a Ph.D. (2024) in Computer Science and Engineering from Instituto Superior Técnico (IST), University of Lisbon, Portugal. She is an Invited Assistant Professor at Lisbon University Institute (ISCTE-IUL) and a member of the Interactive Technologies Institute (ITI) research unit of the Laboratory of Robotics and Engineering Systems (LARSyS). She is a member of the MEROP research team and has participated in the Portuguese contribution in the Analog Mars Missions AMADEE-20 and AMADEE-24 organized by ÖWF. She is currently a Pos-Doc in the SYNTECS project funded by the European Union, and the PI for ARTOp.Inclusive project funded by FCT. Her work has been published at venues, such as ACM SAP, ACM HRI, ACM UIST, INTERACT, IEEE RO-MAN. Her current research interests include human–robot interaction, teleoperation, multimodal interfaces, human factors, accessibility and haptic interfaces.

JOSÉ LUÍS SILVA holds a Ph.D. (2012) in Computer Science from the Portuguese MAP-i Consortium (University of Minho, University of Aveiro and University of Porto). He is an Assistant Professor at Lisbon University Institute (ISCTE-IUL) and a member of the Interactive Technologies Institute (ITI) research unit of the Laboratory of Robotics and Engineering Systems (LARSyS). He is co-leading the MEROP research team, has participated in national and international research projects (including with Airbus and the European Space Agency), and in the Portuguese contribution to Simulated Mars Missions: AMADEE-20 and AMADEE-24 organized by the Austrian Space Forum. He is member of the, ACM Europe Technology Policy Committee, and IFIP TC 13 - Working Group 13.2. His work has been published in prestigious peer-reviewed international journals and conferences such as IEEE Access, Elsevier IJHCS, ACM EICS, ACM IUI and ACM/IEEE HRI. His main research interests lie in Human-Robot Interaction, Interactive Systems and Space Exploration. His main awards and honors include ISCTE-IUL Scientific Awards and a Ph.D. Award from Fraunhofer Portugal Challenge.

This work is licensed under a Creative Commons Attribution 4.0 License. For more information, see https://creativecommons.org/licenses/by/4.0/

This article has been accepted for publication in IEEE Access. This is the author's version which has not been fully edited and
content may change prior to final publication. Citation information: DOI 10.1109/ACCESS.2026.3749135

RODRIGO VENTURA is a tenured Associate Professor of the Electrical and Computer Engineering Department of Instituto Superior Técnico (IST), University of Lisbon, and a senior researcher of the Institute for Systems and Robotics (ISR-Lisbon), part of the Laboratory of Robotics and Engineering Systems (LARSyS), where he coordinates the Space and Aeronautics thematic line. He is the coordinator of the Minor in Space Sciences and Technologies at IST, and of the Master of Business Engineering (MBE) in Space Systems, also at IST. He is Adjunct Faculty of the International Space University (ISU) global faculty, collaborating regularly with ISU in various academic activities. His research is primarily focused on the application of robotics and artificial intelligence to the space domain, including human-robot interaction, mobile manipulation, autonomous navigation, decision making under uncertainty, and machine learning. His activities in space have included robotic experiments on the International Space Station (ISS), using the NASA Astrobee robots, and the participation on various analog space exploration missions (OeWF AMADEE-20 and AMADEE-24). He is associate editor of the Journal of Field Robotics, and member of the AAAI and IEEE associations.

This work is licensed under a Creative Commons Attribution 4.0 License. For more information, see https://creativecommons.org/licenses/by/4.0/